# Chapter 2
# Transient Chaos in Low-Dimensional Systems

We study low-dimensional dynamical systems, i.e., systems described by one-dimensional noninvertible or two-dimensional invertible maps. For such systems it is often possible to obtain analytic understanding of generic properties of transient chaos that are shared by more realistic physical systems. For example, for a higher-dimensional system, one-dimensional maps can be used to model the dynamics along the unstable manifold [220, 564].

For one-dimensional maps, we shall analyze in detail the relation between the natural and the conditionally invariant measures of repellers, and introduce analytic tools based on the Frobenius–Perron type of *eigenvalue equations*. These considerations allow us to derive explicit dimension and entropy formulas. We will also elaborate the relevance of transient chaos to problems in mathematics, physics, and engineering, and address the issue of nonhyperbolicity. In particular, we will show that nonhyperbolic dynamics can lead to a power-law decay, and to the concentration of the natural measure on a single point, despite the fractal character of the repeller.

Two-dimensional invertible maps are equivalent to three-dimensional flows and can be obtained by the standard technique of stroboscopic or Poincaré surface of section [564]. We shall discuss again the relation between the natural and the c-measures, derive the corresponding entropy and dimension formulas, and provide an information-theoretic motivation. A fundamental feature of any chaotic set is the existence of an infinite number of unstable periodic orbits. We will discuss how transient chaos is organized about the periodic orbits. While chaotic saddles are often hyperbolic, meaning that the stable and the unstable manifolds do not become tangent to each other (i.e., there are no homoclinic or heteroclinic tangencies), nonhyperbolic chaotic saddles can also arise [454].

For completeness, the multifractal formalism, a more systematic characterization of the natural measure, will be discussed briefly in Appendix A.

Y.-C. Lai and T. Tél, *Transient Chaos: Complex Dynamics on Finite-Time Scales*,
Applied Mathematical Sciences 173, DOI 10.1007/978-1-4419-6987-3_2,

## 2.1 One-Dimensional Maps, Natural Measures, and c-Measures

### 2.1.1 Basic Properties of One-Dimensional Maps Generating Transient Chaos

Strong dissipation leads to significant contraction in the phase space and consequently to an approximately one-dimensional discrete map on a stroboscopic or Poincaré plane. One-dimensional maps are typically noninvertible. They are the simplest class of dynamical systems in which transient chaos can occur, and insights obtained from studying them can often be useful for exploring transient chaos in higher-dimensional systems.

Let $f(x)$ be a one-dimensional noninvertible map. Transient chaos occurs if an interval $I$ is mapped partially *outside* itself. We shall consider here single-humped map functions, as illustrated by Fig. 2.1. There is a primary escape interval $I_0$ that is mapped outside $I$ in a single iterate. The dynamics of the map outside $I$ is irrelevant. For example, there can be one or more attractors far away, but if there is no feedback from these regions onto $I$, the transient chaotic behavior is completely specified by the function $f$ defined *on* $I$.

As an illustrative example, we consider the classical logistic map $x_{n+1} = f(x_n, r) = rx_n(1-x_n)$, which generates transient chaos for $r > 4$. There is a chaotic repeller in the unit interval $I = (0,1)$, and this interval can be chosen as the restraining region $\Gamma$. Figure 2.2 shows the approximate invariant measure on the repeller for $r = 4.03$ covered by uniform boxes of size $\varepsilon = 2 \cdot 10^{-3}$, where the box probabilities $P_i(\varepsilon)$ are displayed. Figure 2.2 also contains information about the repeller's structure. For example, it can be noticed that the crudest approximation to the

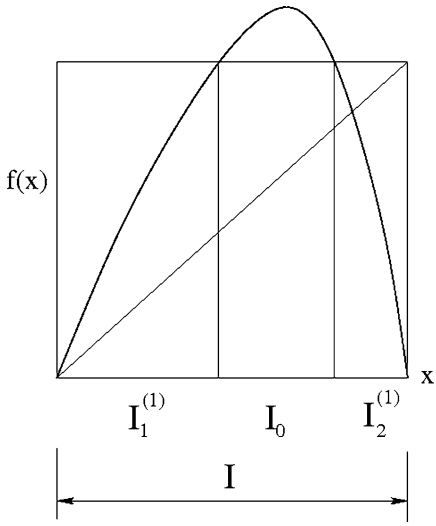


**Fig. 2.1** A typical one-dimensional map generating transient chaos on some interval $I$. Note that points lying outside the two subintervals $I_1^{(1)}$ and $I_2^{(1)}$ escape $I$ after one time unit. Points that do not exit in $n$ steps are contained in the $(n-1)$th preimages of the two subintervals (i.e., in the $n$th preimages of $I$), and exhibit chaotic behavior on time scale $n$ due to the global expansivity of the map

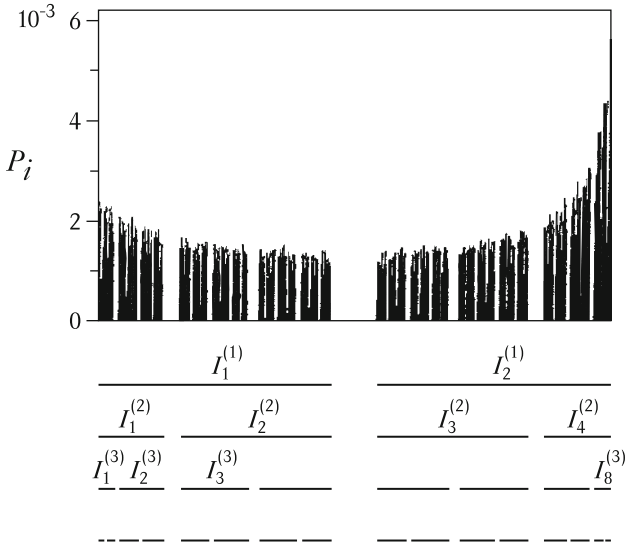


**Fig. 2.2** Natural distribution for the logistic map $x_{n+1} = rx_n(1-x_n)$ for $r = 4.03$ obtained by the ensemble method (cf. Sect. 1.2.2.2) on a grid of size $\varepsilon = 0.002$. The number of initial points distributed uniformly in $I = R = \Gamma$ is $N_0 = 10^7$, and the first 10 and the last 30 steps of trajectories are discarded. The truncated trajectories contain about $10^6$ points, so that reasonable statistics can be obtained. The escape rate can be estimated by comparing the number of trajectories of length 10 and 30 in $I$, which yields, via (1.6), $\kappa \approx 0.07$. The lower part of the figure illustrates the organization of the repeller, where $I_i^{(n)}$ denotes the cylinders at level $n$, i.e., the $n$th preimages of $I = (0,1)$ (cf. Fig. 2.3), and resembles the construction of a Cantor set

repeller cover consists of two intervals, the two preimages $I_1^{(1)}$ and $I_2^{(1)}$ of $I$. At the next stage, each of them splits into two smaller intervals. Subsequent successive refinements will then yield a complete *hierarchy*, the $n$th level of which contains all the $n$th preimages of $I$. The preimage intervals are called *cylinders* and are denoted by $I_i^{(n)}$, where the subscript $i$ enumerating them runs, at the $n$th level, up to $2^n$. Note that here, the base 2 is due to the two branches that the inverse map $f^{-1}$ exhibits. Also note that the cylinders provide coverage of the repeller with *nonuniform* boxes that fit the repeller's structure in a natural manner. An equivalent way of defining the cylinders is to consider the $n$-fold iterated map $f^n$, whose graph contains $2^n$ branches (Fig. 2.3). The intervals mapped exactly onto $I$ by the $n$th iterated map are nothing but the cylinders of level $n$, indicating that points in any subinterval $I_i^{(n)}$ do not leave the restraining region $I$ sooner than $n+1$ steps. Since the folds with derivatives smaller than unity are, for sufficiently large $n$, outside $I$, the dynamics are *expansive*, or in this one-dimensional case, are *hyperbolic* on the repeller.

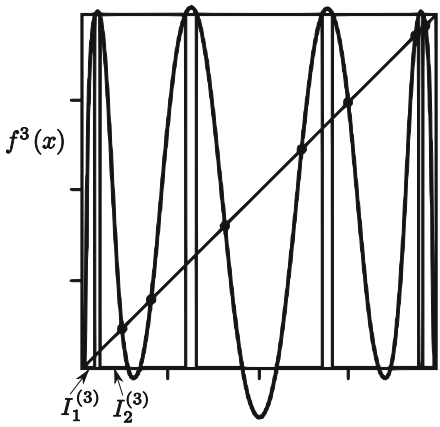


**Fig. 2.3** The threefold iterated logistic map for $r = 4.03$, and cylinders $I_i^{(3)}, i = 1, \ldots, 8$. The *dots* denote points of 3-cycles

### 2.1.2 Conditionally Invariant Measure

We now consider the *conditionally invariant* (c-)measure [596] for one-dimensional maps. This measure is defined on any region $\Gamma$ containing the repeller, and describes how trajectories escape this region. For simplicity we take $\Gamma = I$. Consider the conditional probability that a given region is visited by trajectories originated from random initial conditions in $I$ that do not escape $I$ in $m$ steps. A fraction of these trajectories will escape at the next time step, and hence their last points in $I$ are in the gaps among the cylinders. The conditional probability is thus defined on the *entire* interval $I$. The limit to which this conditional probability converges for $m \to \infty$ is the conditionally invariant measure. As mentioned in Sect. 1.2.3.2, the c-measure is effectively the time-independent distribution maintained by supplying new points into the system exactly according to the escape rate.

The density of the c-measure can be constructed from trajectories of minimal length $m$ in the basic interval. For example, one can select trajectories whose first $m$ points are disregarded and all the remaining points are kept before escaping $I$. This procedure usually converges exponentially fast for rather arbitrary choice of $m$ (e.g., $m = 10$), as exemplified by Fig. 2.4. It can be seen that the measure has a *smooth density* everywhere on the interval $I$, due to the fact that it is in general smooth along the unstable manifold (cf., e.g., Fig. 1.11).

To connect the conditionally invariant measure with the natural measure, we *restrict* the density of the c-measure to cylinders of level $n$. This requires a renormalization so that the total measure on the cylinders is unity. The c-measure $\mu_{ci}^{(n)}$ of intervals $I_i^{(n)}$ characterizes then the motion of trajectories visiting the cylinders of level $n$. For sufficiently large $n$, these are the trajectories exhibiting long-lived chaotic transients. Therefore, the limit of the cylinder measures $\mu_{ci}^{(n)}$ for $n \to \infty$ can be considered as the *exact* natural measure $\mu$ on the repeller:

$$\mu_{ci}^{(n)} \to \mu_i^{(n)}. \tag{2.1}$$

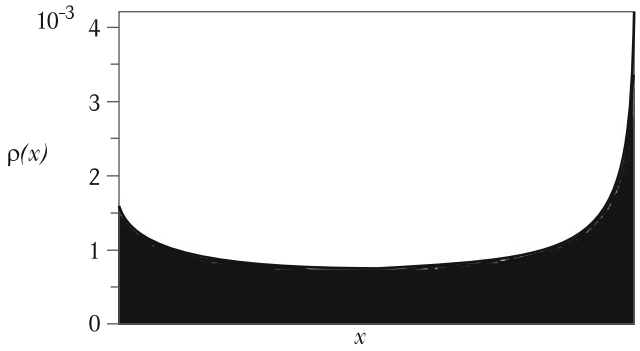


**Fig. 2.4** Density $\rho(x)$ of the conditionally invariant measure for the logistic map on $I = (0, 1)$, obtained by discarding the first 10 steps of trajectories and keeping all points that stay inside the restraining region $I$. Parameter, initial conditions, and the box size $\varepsilon$ are the same as in Fig. 2.2

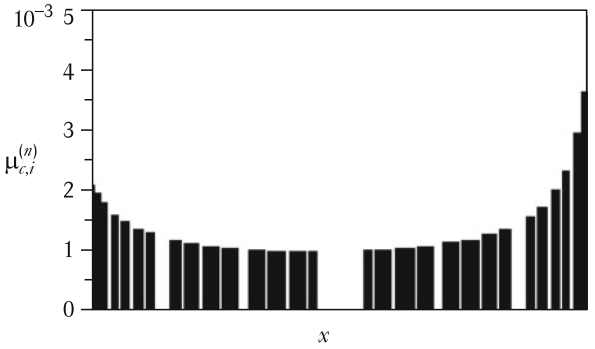


**Fig. 2.5** Measure obtained by restricting the conditionally invariant measure of Fig. 2.4 to cylinders of level $n = 5$ specified by the accuracy $\varepsilon = 0.002$. The cylinder measures in this approximation are $\mu_i^{(5)}$, for $i = 1, \ldots, 32$. Note that the two outermost cylinders are not resolved by the grid

For large $n$ we can omit the subscript $c$ and denote the cylinder measure by $\mu_i^{(n)}$. We thus have two different approximations to the natural measure: the box probabilities $P_i(\varepsilon)$ and $\mu_i^{(n)}$. The equivalence of the two quantities is illustrated in Fig. 2.5, which displays the c-measure restricted to cylinders of level 5. Alternatively, one can smooth out the approximate natural measure shown in Fig. 2.2 on the same set of cylinders. The resulting distribution is essentially the same as that of $\mu_i^{(n)}$ even for the relatively low value of $n = 5$.

### *2.1.3 The Frobenius–Perron Equation*

The Frobenius–Perron equation provides a framework from which analytic insights into the density $\rho(x)$ of the c-measure can be obtained. In general, the equation

governs the time evolution of a density $\rho_n(x)$ via an iterative scheme. For a one-dimensional map exhibiting transient chaos, the equation is

$$\rho_{n+1}(x') = R \sum_{x \in f^{-1}(x')} \frac{\rho_n(x)}{\mid f'(x) \mid}, \tag{2.2}$$

where $R$ is a prefactor and the summation is taken over the preimages of $x'$. For $R = 1$, the equation is the Frobenius–Perron equation for attractors [220, 564], corresponding to a situation without escape. For transient chaos, escapes can be taken into account by choosing properly the prefactor $R$. In particular, by iterating any smooth, positive initial function $\rho_0(x)$ on $I$, the series $\rho_n(x)$ either diverges or tends to zero unless we choose [596, 764]

$$R = \mathrm{e}^{\kappa}, \tag{2.3}$$

which is the compensation factor described in Sect. 1.2.3.2 with $\kappa$ being the escape rate. With this choice of $R$, the series $\rho_n(x)$ converges to a finite $\rho(x)$:

$$\rho_n(x) \to \rho(x) \tag{2.4}$$

*independently* of the choice of the initial function. The limit $\rho(x)$ is the *density* of the c-measure and satisfies the following self-consistent equation:

$$\rho(x') = \mathrm{e}^{\kappa} \sum_{x \in f^{-1}(x')} \frac{\rho(x)}{\mid f'(x) \mid}. \tag{2.5}$$

This equation can be considered as an eigenvalue problem of the Frobenius–Perron, or transfer, operator $\sum_{x \in f^{-1}(x')} \mid f'(x) \mid^{-1}$. The fact that its largest eigenvalue $\exp(-\kappa)$ is less than unity is the mathematical reason for the long-term exponential decay of the survival probability (1.8).

In numerical experiments where the escape rate $\kappa$ is not known a priori, different values for $R$ can be chosen and tested until convergence in $\rho(x)$ is achieved. For transient chaos in typical one-dimensional maps, the convergence is usually quite fast and the limiting $\rho(x)$ of reasonable accuracy can be achieved after a few iterations [764], as shown by one example in Fig. 2.6. In this case, both the escape rate and the density can be found by numerically solving the eigenvalue problem.

In general, the escape rate can be obtained as an integral of density $\rho$ over the intervals $I_1^{(1)}$, $I_2^{(1)}$ (see Fig. 2.1 and (1.14)) not escaping within a single step:

$$\mathrm{e}^{-\kappa} = \mu_{\mathrm{c}}(f^{-1}(I)) \equiv \int_{I_1^{(1)}} \rho(x)\mathrm{d}x + \int_{I_2^{(1)}} \rho(x)\,\mathrm{d}x, \tag{2.6}$$

provided that the c-measure is normalized to unity on $I$: $\int_I \rho(x)\,\mathrm{d}x = 1$. As a consequence, the escape rate can also be expressed by the c-measure of the primary escape interval $I_0$,

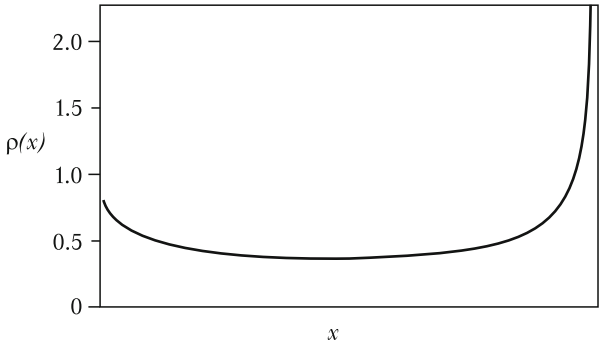


**Fig. 2.6** Density $\rho(x)$ of the logistic map on $I$ for $r = 4.03$, obtained from (2.2) as the eighth iterate of a constant initial function. The relative error is about $10^{-3}$

$$1 - \mathrm{e}^{-\kappa} = \int_{I_0} \rho(x)\,\mathrm{d}x. \tag{2.7}$$

When the escape rate is small so that the approximation $\exp(-\kappa) \approx 1 - \kappa$ holds, we have

$$\kappa = \int_{I_0} \rho(x)\,\mathrm{d}x \approx \rho(x_c)L, \tag{2.8}$$

where $L$ is the size of $I_0$. The approximate equality expresses that for small $\kappa$ the primary escape interval is short, and the integral over $I_0$ can then be approximated as the density about a typical point $x_c$ in $I_0$ multiplied by the length $L$ of the escape interval.

By iterating (2.2), one can see the presence of a singularity at the maximum of $f(x)$, but it falls *outside* $I$. This supports again the view that the density of the c-measure is a smooth function on close neighborhoods of hyperbolic repellers. Using the definition of the density, the cylinder measure $\mu_i^{(n)}$ can be expressed as

$$\mu_i^{(n)} = \frac{\int_{x \in I_i^{(n)}} \rho(x)\,\mathrm{d}x}{\sum_j \int_{x \in I_j^{(n)}} \rho(x)\,\mathrm{d}x}. \tag{2.9}$$

The smoothness of $\rho$ enables us to obtain the actual value of the density from the integrals, for sufficiently small cylinders. Since the density does not change with the refinement, the asymptotic scaling with $n$ is governed by the length scales only. Thus, for large $n$, *the measure of a cylinder is proportional to its length*. More precisely, we have

$$\mu_i^{(n)} \sim \frac{\varepsilon_i^{(n)}}{\sum_j \varepsilon_j^{(n)}} \quad \text{for } n \gg 1, \tag{2.10}$$

where $\varepsilon_i^{(n)}$ stands for the length of the cylinder $I_i^{(n)}$. The $n$-independent proportionality factor not written out here depends on the actual form of $\rho$. Equation (2.10)

is essential for our subsequent discussions. Note that the total length of cylinders at level $n$ is proportional to the number of points not yet having escaped $I$ after $n$ steps. The cylinder measure can therefore be expressed as

$$\mu_i^{(n)} \approx \mathrm{e}^{\kappa n} \varepsilon_i^{(n)}. \tag{2.11}$$

## 2.2 General Relations

There exist general relations in simple form among the metric entropy, the Lyapunov exponent, the information dimension, and the escape rate. The box-counting dimension and the topological entropy, however, can be related to the escape rate in a more complicated manner only. We shall derive these relations in this section.

### *2.2.1 Lyapunov Exponent, Information Dimension, and Metric Entropy*

With each cylinder $I_i^{(n)}$, one can associate a unique symbol sequence $\{S_j\}$ ($j = 1,2,\ldots,n$) of length $n$. In a single-humped map, the symbols are binary: $S_j$ takes on the value 0 (1) if a trajectory started in the cylinder is at time step $j-1$ in the subinterval $I_1^{(1)}$ ($I_2^{(1)}$) (see Fig. 2.1). The leftmost and the rightmost cylinders have the code $\{0,0,\ldots,0\}$ and $\{1,0,\ldots,0\}$, respectively. The cylinders can then be labeled by the corresponding symbol sequences. Moreover, the cylinder measures are exactly the path probabilities $P(\{S_j\})$ (1.24) for finding a symbolic trajectory $\{S_j\}$ of length $n$:

$$\mu_i^{(n)} = P(\{S_j\}). \tag{2.12}$$

To obtain the Lyapunov exponent, one observes that the logarithm of the slope of the $n$-fold iterated map $f^n$ at $x$ is just the stretching factor (see Sect. 1.2.3.3) at this point. The slope is, however, approximately constant in a cylinder, as illustrated by Fig. 2.3. Since the length of $I$ can, in general, be chosen to be unity, the stretching factor in cylinder $I_i^{(n)}$ of size $\varepsilon_i^{(n)}$ is approximately $1/\varepsilon_i^{(n)}$. The stretching exponent is then $\Lambda_{1i}(n) = -\ln \varepsilon_i^{(n)}$. The average Lyapunov exponent (1.18) is given by

$$\lambda_1 = \frac{1}{n}\sum_i \Lambda_{1i}^{(n)} \mu_i^{(n)} = -\frac{1}{n}\sum_i \varepsilon_i^{(n)} \mathrm{e}^{\kappa n} \ln \varepsilon_i^{(n)} \tag{2.13}$$

for $n \gg 1$. The metric entropy from (1.24), according to (2.11), and (2.12), is

$$K_1 = -\frac{1}{n}\sum_i \varepsilon_i^{(n)} \mathrm{e}^{\kappa n} \left(\kappa n + \ln \varepsilon_i^{(n)}\right). \tag{2.14}$$

Comparing (2.13) and (2.14), we obtain

$$K_1 = \lambda_1 - \kappa. \tag{2.15}$$

This indicates that for a chaotic repeller of a one-dimensional map, the metric entropy $K_1$ is *not* equal to the Lyapunov exponent (in contrast to the situation of a chaotic attractor, where the two are equal [220, 564]), with the difference being the escape rate.

The information dimension of the repeller can be calculated using the probabilities $P_i = \mu_i^{(n)}$ in (1.22). A straightforward substitution of $P_i$ in (1.22) yields

$$D_1 = 1 - \frac{\kappa}{\lambda_1}. \tag{2.16}$$

We see that the information dimension of the natural distribution on a chaotic repeller is always less than unity. The difference is given by the ratio of two rates: the escape rate and the Lyapunov exponent. In addition, since $D_1$ is nonnegative, we have

$$\kappa \leq \lambda_1, \tag{2.17}$$

where the equality holds only for point repellers whose natural distribution is concentrated in a point ($D_1 = 0$). A chaotic repeller is thus globally *less* repelling than typical points in it, since the escape rate is smaller than the average Lyapunov exponent. It may be said that the fractal structure tends to "stabilize" the repeller because a larger dimension implies generally slower escape.

Finally, from (2.15) and (2.16), we obtain

$$K_1 = \lambda_1 D_1. \tag{2.18}$$

The metric entropy is thus the product of the Lyapunov exponent and the information dimension. Equations (2.15), (2.16), and (2.18) are particular instances of the general relations expressed by (1.29) and (1.30).

### 2.2.2 Box-Counting Dimension and Topological Entropy

The idea behind the Frobenius–Perron equation (2.5) can be exploited for calculating the box-counting dimension. In particular, note that in fitting a smooth curve to the natural distribution on a grid of size $\varepsilon \ll 1$ such as the one in Fig. 2.2, one finds that its form $\tilde{\rho}(x)$ differs from the density $\rho(x)$ of the c-measure. The reason is that the cylinders of level $n \gg 1$ are by far not of equal size. It is possible to find an equation of the type of the Frobenius–Perron equation (2.5) whose solution is $\tilde{\rho}(x)$.

Consider the coarse-grained chaotic repeller specified on a grid of fine resolution $\varepsilon$. Take an interval of length $\Delta x \ll 1$ within $I$ that is much larger than $\varepsilon$. The probability of finding a point on the repeller within the interval of length $\Delta x$ is

$N(\varepsilon)\varepsilon/\Delta x$, where $N(\varepsilon)$ is the number of bins of size $\varepsilon$ covering the repeller inside $\Delta x$, and $N(\varepsilon)\varepsilon$ is the total length of such bins. By the definition of the box-counting dimension (1.19), this quantity scales with $\varepsilon$ as $\varepsilon^{1-D_0}$. The probability that a point of the image interval $\Delta x' = f'(x)\Delta x$ belongs to the repeller is $N(\varepsilon\Delta x/\mid \Delta x'\mid)\varepsilon/\mid \Delta x'\mid$, since the map is locally linear over the interval of length $\Delta x$, and a longer interval $\Delta x'$ corresponds to using a finer resolution $\varepsilon\Delta x/\Delta x'$ in $N$. After one iterate, the probability of being on the repeller has changed by a factor of $\mid \Delta x/\Delta x'\mid^{1-D_0}$, which is typically less than unity. A *local* escape rate $\kappa(x)$ can thus be defined as

$$\mathrm{e}^{\kappa(x)} = \mid f'(x)\mid^{1-D_0}. \tag{2.19}$$

The decrease of the probability from a coarse-grained repeller accompanying the escape process can be compensated by multiplying the probability of being on the repeller by $\exp[\kappa(x)]$ for every point $x$. In an equation analogous to (2.2), there is then no overall correctional factor $R$, but the exponent of the derivative changes from unity to $D_0$. These considerations lead to [753]

$$\tilde{\rho}_{n+1}(x') = \sum_{x\in f^{-1}(x')} \frac{\tilde{\rho}_n(x)}{\mid f'(x)\mid^{D_0}}, \tag{2.20}$$

which we call the *dimension equation*. By iterating any smooth, positive initial function $\tilde{\rho}_0(x)$ on $I$, one can find convergence to a finite density if the exponent is chosen to be the repeller's box-counting dimension. Equation (2.20) is a kind of eigenvalue equation for the dimensions, and it provides a fast numerical algorithm for determining $D_0$. For our example in Fig. 2.2, the calculation yields $D_0 = 0.905344$. The series of $\tilde{\rho}_n(x)$ converges to the density $\tilde{\rho}(x)$, a smooth covering curve for the *natural* distribution on the repeller *coarse-grained* on a uniform grid [753].

Similar types of equations exist for the information dimension and other quantities, as shown in Appendix A (A.12). Using a cumulant expansion of the local Lyapunov exponents applied to these equations, one finds a relation between the box-counting dimension and these cumulants in the form of

$$\kappa = (1-D_0)\lambda_1 + \frac{1}{2}(1-D_0)^2 Q_2 + \cdots, \tag{2.21}$$

where $Q_2$ is the second cumulant. An analogous relation for the topological entropy [380] can be obtained, which is

$$K_0 = \lambda_1 - \kappa + \frac{1}{2}Q_2 + \cdots, \tag{2.22}$$

as also derived in Appendix A. Equations (2.21) and (2.22) show that, in contrast to $D_1$ and $K_1$, the box-counting dimension and the topological entropy can be related to the escape rate only if an infinite series containing the cumulants of the local Lyapunov exponents is also taken into account.

Since all possible binary sequences are allowed to occur in the class of maps in Fig. 2.1 (there are $\Omega_m = 2^m$ sequences of length $m$), the topological entropy from (1.25) is

$$K_0 = \ln 2, \tag{2.23}$$

regardless of the particular form of $f(x)$.

### 2.2.3 An Analytically Tractable Example: The Tent Map

As an analytic example, we consider the tent map defined on the unit interval $I = (0,1)$:

$$f(x) = \begin{cases} ax & \text{for } x < b/(a+b), \\ b(1-x) & \text{for } x > b/(a+b), \end{cases} \tag{2.24}$$

where $a > 1$ and $b > a/(a-1)$. The lengths of the two subintervals $I_1^{(n)}$ and $I_2^{(n)}$ (cf. Fig. 2.1) are $1/a$ and $1/b$, respectively. For the tent map, the convergence of an initial distribution $\rho_0(x)$ to the density of the c-measure can be followed explicitly under the Frobenius–Perron equation (2.2):

$$\rho_{n+1}(x') = R\left(\frac{\rho_n(x'/a)}{a} + \frac{\rho_n(1-x'/b)}{b}\right). \tag{2.25}$$

To find a solution to (2.25), we assume that the distribution is linear at any iteration:

$$\rho_n = \alpha_n x + \beta_n. \tag{2.26}$$

A direct substitution yields the following mapping for the coefficients:

$$\alpha_{n+1} = R\left(\frac{1}{a^2} - \frac{1}{b^2}\right)\alpha_n, \quad \beta_{n+1} = R\left(\frac{1}{a} + \frac{1}{b}\right)\beta_n + \frac{R}{b}\alpha_n. \tag{2.27}$$

A finite nonzero limiting value of $\beta$ exists only if the factor in front of $\beta_n$ is unity, which gives $R(1/a + 1/b) = 1$. The escape rate is thus given by

$$\kappa = \ln R = -\ln(1/a + 1/b) = \ln a + \ln b - \ln(a+b). \tag{2.28}$$

With this value of $R$, the factor in front of $\alpha_n$ is less then unity in modulus, and hence the series of $\alpha_n$ converges to zero, so that the asymptotic distribution is a constant. Taking into account normalization, we obtain $\rho(x) \equiv 1$.

Applying (2.20) also yields a constant asymptotic density $\tilde{\rho}$, provided that the box-counting dimension satisfies[1]

$$a^{-D_0} + b^{-D_0} = 1. \tag{2.29}$$

Due to the strict self-similarity of the cylinder construction, other dynamical invariants can be found from the first level. In particular, since $\rho = 1$, the first-level cylinder measures are $\mu_1^{(1)} = b/(a+b)$ and $\mu_2^{(1)} = a/(a+b)$ with local slopes $a$ and $b$ on these cylinders, respectively. From (2.13) we obtain

$$\lambda_1 = \frac{a\ln b + b\ln a}{a+b}. \tag{2.30}$$

For the metric entropy (2.14), we have

$$K_1 = -\frac{a\ln a + b\ln b}{a+b} + \ln(a+b). \tag{2.31}$$

From (1.22), the information dimension of the natural measure of the repeller is

$$D_1 = \frac{-a\ln a - b\ln b + (a+b)\ln(a+b)}{a\ln b + b\ln a}. \tag{2.32}$$

One can see that indeed, the general relations (2.15), (2.16), and (2.18) are non-trivially satisfied for the tent map. It is only for the symmetric case $a = b$ that the dimensions are equal to each other, and so are the entropies. In particular, in this case we have $D_0 = D_1 (= \ln 2/\ln a)$ and $K_0 = K_1 (= \ln 2)$.

## 2.3 Examples of Transient Chaos in One Dimension

The following examples, taken from different disciplines including number theory, engineering, and statistical mechanics, illustrate the ubiquity of transient chaos.

### *2.3.1 Numbers with Incomplete Continued Fractions*

It is known that every positive number $x$ can be expanded in a unique continued fraction [331, 408], i.e., the number can be written as

[1] The same result follows for arbitrary choices of the initial densities, and the constant-valued distribution is indeed an attractor of the functional recurrences (2.2) and (2.20).

$$x = \cfrac{1}{i_1 + \cfrac{1}{i_2 + \cfrac{1}{i_3 + \cdots}}}, \tag{2.33}$$

where the $i_k$ are natural numbers. The expansion is obtained by subtracting from the reciprocal of the number the integer part ($i_1$) of the reciprocal, then taking the resulting reciprocal and subtracting from it its integer part ($i_2$), and so on.

The one-dimensional Gauss map[2] defined on $I = (0, 1]$ as the difference between the reciprocal and its integer part is

$$x_{n+1} = f(x_n) \equiv \frac{1}{x_n} - \left[\frac{1}{x_n}\right]. \tag{2.34}$$

The map is related to continued fractions. In particular, it contains infinitely many branches; see Fig. 2.7a. Starting the counting from the rightmost branch as branch $f_1$, branch $i$ is of the form $f_i(x) = 1/x - i$ and is defined over the interval $(1/(i+1), 1/i)$. Taking an initial point $x_0$ in this interval, we obtain $x_1 = 1/x_0 - i$ and hence $x_0 = 1/(i + x_1)$. The number $x_1$ can thus be considered as the remnant after a single step of the continued fraction expansion. The expansion can be continued. For example, taking an initial point $x_0$ mapped by $f_{i_1}$ first and then by $f_{i_2}$, we get

$$x_0 = \cfrac{1}{i_1 + \cfrac{1}{i_2 + x_2}}. \tag{2.35}$$

A comparison with (2.33) shows that the sequence $i_1, i_2, i_3, \ldots$ of branch indices encountered while iterating map (2.34) with any irrational initial condition $x_0$ corresponds precisely to the infinite continued fraction expansion of $x_0$. Accordingly,

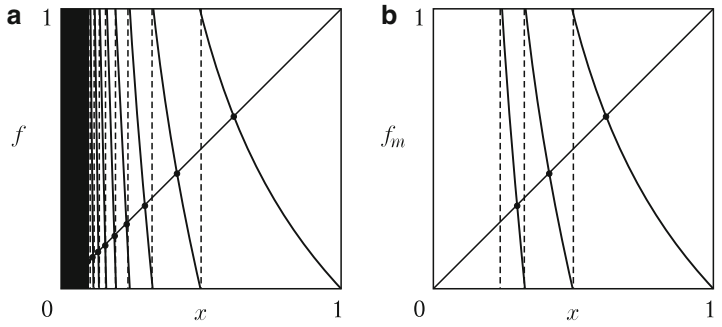


**Fig. 2.7** (**a**) Gauss map $f$ and (**b**) truncated Gauss map $f_m$ that contains only branches with $i \leq m$. Here $m = 3$

[2] Gauss was aware of the fact that this map has an invariant density proportional to $1/(1+x)$. The map is in fact chaotic in modern terminology [328].

the fixed point $x_i^*$ belonging to branch $i$ is a number that contains only $i$ in its continued fraction, where $x_1^*$ is in fact the golden mean. Since any number in $(0,1]$ can be expanded if all positive integers can appear in the expansion, the full interval $I=(0,1]$ remains invariant under the map (2.34).

One can, however, ask what the numbers whose continued fractions contain *certain* integers only are. They form fractal subsets of the unit interval. In particular, we shall be interested only in numbers with continued fractions containing integers less than or equal to a certain threshold $m$. These numbers must be *invariant* under the truncated Gauss map $f_m(x_n)$ that is of the same form as (2.34) but does not contain the branches $i=m+1,m+2,\ldots$, as shown in Fig. 2.7b. The truncated map $f_m$ is thus of the form of (2.34) but is defined on the interval $[1/(m+1),1]$ only.

Points from the interval $I_0=(0,1/(m+1))$ have integers larger than $m$ in their expansion. As a result, whenever a point under iteration enters this region, it should be discarded. Map $f_m$ is therefore a map from which escape takes place, generating transient chaos. The numbers with continued fractions containing integers less than or equal to $m$ form the *chaotic repeller* of the map $f_m$. The repellers can be constructed numerically. Several representative repellers are shown in Fig. 2.8.

The box-counting dimension $D_{0m}$ of the repeller of the map $f_m$ follows from the dimension equation (2.20), which now reads

$$\tilde{\rho}_{n+1}(x')=\sum_{i=1}^{m}(x'+i)^{-2D_{0m}}\tilde{\rho}_n\left(\frac{1}{x'+i}\right). \tag{2.36}$$

The values of $D_{0m}$ can be determined from (2.36) numerically, and the results [328] are summarized in Table 2.1. By now, efficient algorithms exist [330,358] for determining these dimensions up to many more digits than shown here. It is interesting to mention that by means of spectral methods, D. Hensley derived [329] an analytic expression for $D_{0m}$, valid for large $m$:

$$D_{0m}=1-\frac{6}{\pi^2 m}-\frac{72\ln m}{\pi^4 m^2}. \tag{2.37}$$

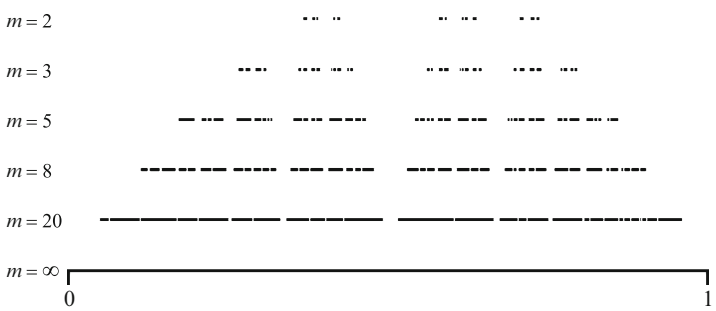


**Fig. 2.8** Numbers of the unit interval with continued fraction expansions containing integers less than or equal to $m$ for $m=2,3,5,8,20$, obtained as invariant chaotic repellers under the map $f_m$. Each set is similar to a Cantor set

**Table 2.1** Box-counting dimension $D_{0m}$ of irrational numbers with continued fraction expansions containing integers less than or equal to $m$

| $m$ | 2 | 3 | 4 | 5 | 6 | 7 | 8 |
|---|---|---|---|---|---|---|---|
| $D_{0m}$ | 0.5313 | 0.7057 | 0.7889 | 0.8368 | 0.8676 | 0.8890 | 0.9046 |

For $m > 8$, this expression is quite accurate: its predicted values agree with the numerically obtained dimension values within less than half of 1%.

### 2.3.2 Shimmying Wheels

The lateral vibrations of towed wheels, the shimmies (called after a dance that was popular back in the early 1920s), are self-excited nonlinear oscillations of great engineering relevance. These vibrations can be observed during the motion of the towed wheels of shopping carts, wheelchairs, trailers, or on the front wheels of airplanes, bicycles, or motorcycles. In the simplest setting, the vehicle can be modeled as a rigid body moving along a straight line at a constant speed $v$. For practical purposes, a stationary rolling of the wheel is desirable so that the wheel's center of mass moves parallel to the towing velocity. Shimmy may occur if some part of the wheel system, either the wheel itself or the point at which it is affixed, is elastic [738].

To gain insight here we consider an idealized model that exhibits shimmying motion [272]. The wheel is assumed to be rigid, but the connecting assembly can move laterally, as shown schematically in Fig. 2.9. The vehicle moves at a constant velocity $v$ along the $x$-axis. The vertical center of rotation of the wheel, the kingpin, is attached to the vehicle via a spring that allows the kingpin to oscillate in the $y$ direction. An important parameter of the system is the caster length $l$, i.e., the offset of the wheel's axis with respect to the kingpin. The deflection angle of the wheel assembly with respect to the $x$-axis is $\psi$; the rotational angle of the wheel is $\phi$. In a reference frame co-moving with the vehicle, the degrees of freedom are the angles $\psi$ and $\phi$, and the instantaneous position $y$ of the kingpin. If the wheel rolls, i.e.,

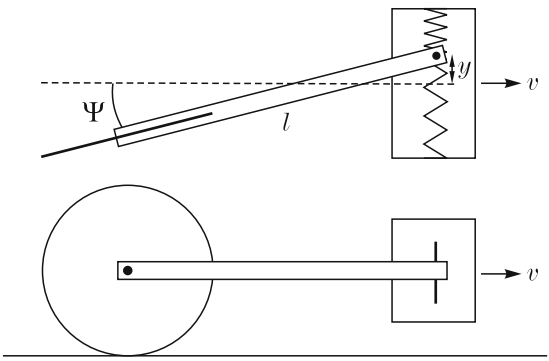


**Fig. 2.9** Schematic diagram of an idealized wheel model that exhibits chaotic shimmying

its contact point has zero velocity relative to the ground, the rotational angle is no longer an independent variable. The system thus has two degrees of freedom, and the phase space is four-dimensional. Note, however, that due to the prescribed towing velocity, the total energy is not conserved; either the system can be dissipative, or it can absorb energy via the constraining force of the vehicle's engine that provides the constant speed.

The state of straight rolling ($\psi = 0$, $y = 0$) is unstable for short caster length for $l < l_c$, where the critical length $l_c$ is determined by other parameters such as the wheel's radius, the masses, and the towing velocity [738]. Even when the caster length is sufficiently long that the system is in the regime of stable straight rolling, the dynamics is nontrivial, since there exists an unstable limit cycle outside the fixed-point attractor at the origin. For vibrations of amplitude larger than that of the limit cycle, the corresponding $\psi$ values increase in time. In this process, the angle of deflection reaches a critical value for which the static friction is no longer able to provide the necessary constraining force for rolling. That is, the wheel *slides*. It is insightful to focus on the dynamics of a sliding wheel for which $\phi$ is a relevant variable, and the phase space becomes six-dimensional. Due to the sliding friction, the dynamics is strongly dissipative, and the velocity of the contact point starts decreasing after some time and sooner or later it approaches zero asymptotically, recovering the rolling state. An essential feature of the full dynamics is thus the temporary change between a four- and a six-dimensional phase space. When a trajectory enters the former, its destination depends on whether it is inside or outside the unstable limit cycle. If it is outside, the amplitude of the $\psi$-oscillations starts growing, the condition of rolling cannot be satisfied, and the trajectory will be in the larger phase space again. Due to such events, the wheel exhibits chaotic "dance" (motion). If, however, a return occurs to some region inside the limit cycle and into the basin of attraction of the fixed-point attractor, the straight rolling of the wheel is approached asymptotically. This actually occurs with a finite probability.

The transiently chaotic shimmying of wheels, occurring for a broad range of parameters, can be represented by an approximately one-dimensional map due to the strong dissipation in the underlying dynamics [739]. On the Poincaré section taken at $y = 0$, the map $\psi_{n+1} = f(\psi_n)$ consists of two branches, as shown in Fig. 2.10. Rolling is represented by the left branch with an unstable fixed point at $\psi^*$ that represents the unstable limit cycle. The critical value at which sliding starts is denoted by $\psi_{sl}$. There is a jump in the dynamics because the right branch corresponding to sliding decreases and stretches somewhat *below* the level of $\psi^*$. The narrow interval $I_0$ is thus the escape interval, and it provides a mechanism for trajectories to return to the attractor at the origin. Insofar as the trajectory is inside the box above $\psi^*$, the dynamics is chaotic. Thus, we conclude that the shimmying motion of wheels can be transiently chaotic for typical parameters, which can indeed be observed, for example, when trolleys at supermarkets or airports are towed. Control of such transient chaotic motions in motorcycles and in airplanes is a basic task in vehicle engineering [738, 754, 755].

A numerical investigation of the transient chaotic dynamics within the interval $(\psi^*, \psi_{\max}) = (6, 9)$ degrees in a realistic case leads to the conclusion that the

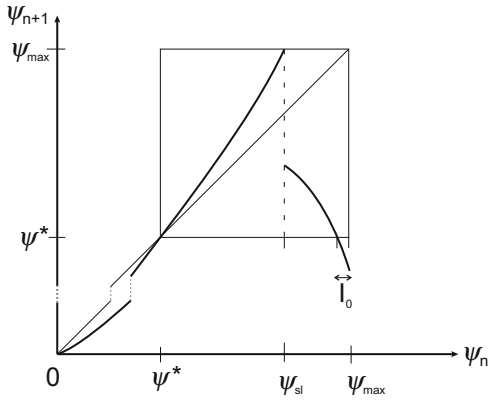


**Fig. 2.10** Schematic diagram of the one-dimensional return map of the deflection angle $\psi$ of a shimmying wheel. The *square* indicates the box within which chaotic dynamics occur. Due to the small gap $I_0$ at its lower right corner, the map is open, and shimmying is transiently chaotic


**Fig. 2.11** Chaotic repeller associated with shimmying motion on the angle interval $(\psi^*, \psi_{\max}) = (6,9)$ degrees

underlying chaotic repeller is rather dense, with box-counting dimension $D_0 \approx 0.95$, as shown in Fig. 2.11. The escape rate is $\kappa \approx 0.006$. Taking into account the characteristic time of oscillations $t_0 = 0.63\,\mathrm{s}$ [739], one can estimate that the average lifetime is $\tau \approx t_0/\kappa = 100\,\mathrm{s}$ (using (1.7)), which is the typical duration of shimmying observed, say, when trolleys are towed.

### *2.3.3 Random-Field Ising Chain*

Take a semi-infinite chain of Ising spins $\{s_1, s_2, \ldots, s_n, \ldots\}$ in an inhomogeneous external field $\{h_1, h_2, \ldots, h_n, \ldots\}$ with the interaction Hamiltonian

$$H = \sum_{j=1}^{\infty} (K s_j s_{j+1} + h_j s_j), \tag{2.38}$$

where $K$ is a coupling constant. For simplicity we use units in which $k_B T = 1$. The set of local fields $\{h_j\}$ is considered a particular realization of a random field distribution assuming at each site the values $+h$ and $-h$ with probabilities $p$ and $1-p$, respectively. The thermodynamic properties are determined by the following partition function:

$$Z = \mathrm{e}^{-F} = \sum_{\{s_1, s_2, \ldots\}} \exp\Big[ -K s_1 s_2 - h_1 s_1 - \sum_{j=2}^{\infty} (K s_j s_{j+1} + h_j s_j) \Big] \tag{2.39}$$

for a fixed realization of the fields $\{h_j\}$ and then by averaging the free energy over different realizations. The summation over spins can be obtained recursively [658]. Since the first spin appears in two terms of $H$ only, the partition function can be evaluated, yielding

$$Z = \sum_{\{s_2,s_3,\dots\}} 2\cosh(Ks_2 + h_1) \exp\left[-\sum_{j=2}^{\infty}(Ks_js_{j+1} + h_js_j)\right]. \tag{2.40}$$

Since $s_2$ can take on the values $\pm 1$ only, an exponential representation of the hyperbolic cosine function gives

$$\cosh(Ks_2 + h_1) = \exp[A(K,h_1) + g(K,h_1)s_2], \tag{2.41}$$

where

$$A(K,x) = \frac{1}{2}\ln[\cosh(K+x)\cosh(K-x)],$$
$$g(K,x) = \frac{1}{2}\ln[\cosh(K+x)/\cosh(K-x)].$$

This form shows that spin 1 contributes an amount $-A(K,h_1)$ to the free energy $F$, and generates simultaneously also an extra field $g(K,h_1)$ for spin 2. The partition sum can thus be rewritten as

$$Z = \sum_{\{s_2,s_3,\dots\}} \exp(A(K,h_1)) \exp\left[-Ks_2s_3 - x_2s_2 - \sum_{j=3}^{\infty}(Ks_js_{j+1} + h_js_j)\right], \tag{2.42}$$

where $x_2$ is an effective field acting on spin 2 and is given by

$$x_2 = h_2 + g(K,h_1). \tag{2.43}$$

Note that the partition sum has a form similar to the original one (with $x_2$ replacing $h_2$). The summation over subsequent spins can then be carried out in an analogous way. After $n$ steps we find the field acting on spin $(n+1)$ as

$$x_{n+1} = h_{n+1} + g(K,x_n), \tag{2.44}$$

and the actual contribution to the free energy becomes $-A(K,x_n)$. As a result, a recurrence can be found that is actually *random*, since the fields $\{h_j\}$ are random variables [302]. According to rule (2.44), the effective field $x_{n+1}$ takes on the values $h + g(K,x_n)$ and $-h + g(K,x_n)$ with probabilities $p$ and $1-p$, respectively. Consequently, the recurrence can be written as a *two-valued* map in which trajectories stay on the upper and lower branches with probabilities $p$ and $1-p$, respectively, as shown in Fig. 2.12. The actual form of the map depends on the coupling constant $K$ and the field magnitude $h$. Although the branches alone are not

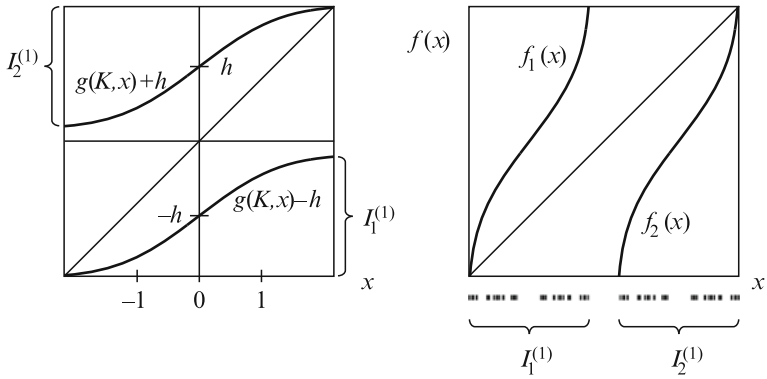


**Fig. 2.12** For a random Ising chain, random map generating the local field $x$ (*left*) and the inverse of the map (*right*). The repeller of this map ($K = 1$, $h = 1.1$) shown at the *bottom* is the attractor of the random iteration (2.44) for any choice of the probability $p$

expanding, the random map exhibits chaotic motion on an *attractor*. The natural invariant measure on this attractor is physically important, since the averaged thermal free energy per spin is just the mean value of $-A(K,x)$ taken with respect to the natural measure of variable $x$ on the attractor. The averaged magnetization per spin and other thermodynamic properties can also be expressed by the natural measure of the attractor [302].

When there is a gap between the branches, as shown in Fig. 2.12, the attractor is a *fractal*. This can be seen by noting that the whole interval $I$ on which the dynamics is defined is mapped into two smaller subintervals $I_1^{(1)}$ and $I_2^{(1)}$ with a gap in between. The images of the small subintervals also have gaps at every level. In fact, these subintervals are exactly the *cylinders* in the *inverted* map $f(x)$ shown in the right panel of Fig. 2.12. It can thus be concluded that the attractor of the random map is nothing but the *repeller* of the inverted map, which holds for all values of $p$. The natural measure on the attractor, however, depends on the choice of $p$ and is not related to the natural measure of the repeller [54]. The former can be obtained by iterating the map $f$ backward with branching probabilities $p$ and $1-p$ and is independent of the choice of the initial point. The attractor geometry (the fractal pattern in Fig. 2.12) and its box-counting dimension ($D_0 = 0.8$), however, follow from the dynamics of the inverted map.

## 2.4 Nonhyperbolic Transient Chaos in One Dimension and Intermittency

Nonhyperbolicity in a one-dimensional map arises when the local slope of the map is unity or infinite, which can lead to escaping dynamics differing from those in hyperbolic systems.

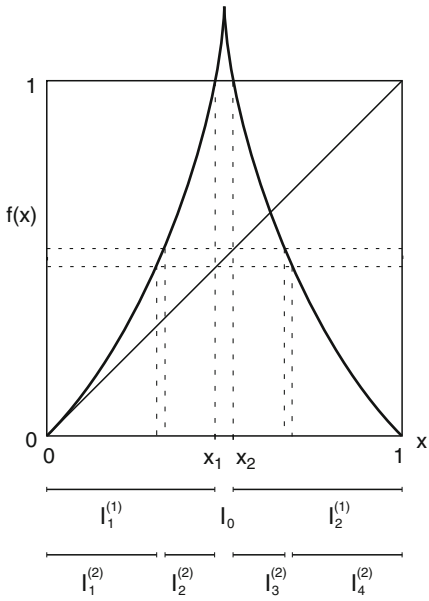


**Fig. 2.13** Symmetric nonhyperbolic map with left branch $f(x) = x + 3x^2$ generating transient chaos. The construction of the first-level *cylinders* is indicated

In particular, the presence of a single marginally stable orbit implies a slow, nonexponential decay process and an intermittent type of behavior before escaping. To illustrate these features, we consider the class of maps shown in Fig. 2.13. About the origin, for $x \ll 1$ the maps are assumed to have the form

$$f(x) = x + Ax^{k-1}, \quad k \geq 3, \tag{2.45}$$

and they are expanding otherwise: $| f'(x) | > 1$. The origin is thus marginally stable, leading to weak repulsion of trajectories that come close to the origin and relatively long dwelling times there. This region can thus be said to be *sticky*. Because of the long dwelling time, iterations of the map can be approximated by a continuous-time differential equation:

$$\frac{\mathrm{d}x}{\mathrm{d}t} = Ax^{k-1}, \tag{2.46}$$

solutions to which indicate that the time $t$ needed to reach a finite distance $l$ from any initial point $x_0$ close to the origin scales as $t \sim {x_0}^{-(k-2)}$. This implies that for a smooth initial distribution, the number $N(n)$ of trajectories staying inside a small interval about the origin changes, after a large number $n$ of iterations, as

$$N(n) \sim n^{-1/(k-2)}. \tag{2.47}$$

As a consequence, the survival probability (see Sect. 1.2.1) also scales as

$$P(n) \sim n^{-1/(k-2)}. \tag{2.48}$$

Its decay follows a power law $n^{-\sigma}$ with an algebraic-decay exponent $\sigma = 1/(k-2)$ for $n \gg 1$, and hence the escape rate is zero: $\kappa = 0$. The cylinder construction shows, however, that the repeller, in fact a nonhyperbolic repeller, is a fractal set of dimension $D_0 > 0$ [161].

We now consider the c-measure. Observe first that for maps having a local form $f(x) \sim 1 - a|\,x - x_i\,|^z$ $(i = 1,2)$ in the vicinities of the internal endpoints $x_i$ of intervals $I_1^{(1)}$, $I_2^{(1)}$, the relation between point $x' \approx 1$ and its preimages $x$ is $x - x_i = (-1)^i[(1-x')/a]^{1/z}$. From the Frobenius–Perron equation (2.5) with $\kappa = 0$, we obtain

$$\rho(x') \sim \left(1 - x'\right)^{1/z-1} \quad \text{for } x' \to 1. \tag{2.49}$$

Note that for maps of the type in Fig. 2.13, $z = 1$ and $\rho(x')$ tends to a constant for $x' \to 1$. The Frobenius–Perron equation (2.5) for $x' \to 0$ becomes

$$\rho(x') = \frac{\rho(x)}{1 + (k-1)Ax^{k-2}} + \frac{\rho(1)}{|\,f'(1)\,|}. \tag{2.50}$$

Since in this regime $x' \approx x$, the equation can be satisfied only if $\rho(x')x'^{k-2} = \text{const}$, i.e.,

$$\rho(x') \sim x'^{-(k-2)} \quad \text{for } x' \to 0. \tag{2.51}$$

The density of the c-measure is *singular* at the origin, implying that the c-measure $\mu_1^{(n)}$ of the leftmost cylinder is much larger than any other $\mu_i^{(n)}$ at level $n$. Since the length $\varepsilon_1^{(n)}$ shrinks with $n$ much more slowly than that of the others, in the asymptotic limit the full measure is concentrated at the origin: $\mu_1^{(\infty)} = 1$. The natural measure of this nonhyperbolic repeller can thus be represented by a Dirac delta function situated at the origin. As a consequence, the information dimension is $D_1 = 0$, and the average Lyapunov exponent is that of the origin, i.e., $\lambda_1 = 0$. The repeller is therefore nonchaotic in the sense of zero Lyapunov exponent, but strange since it is fractal. It has therefore been called a *strange nonchaotic repeller* [161] (in analogy with strange nonchaotic attractors [241]). Trajectories spend long times near the origin, but burst into other regions of the repeller from time to time, return to the origin again, and so on. The dynamics is thus *intermittent* [612] before escape takes place.

In the case of nonhyperbolicity due to infinite derivatives, $z < 1$ at the endpoints $x_1, x_2$ of the primary escape interval, so the density vanishes at $x' = 1$, as indicated by (2.49). The Frobenius–Perron equation about the origin reads

$$\rho(x') = R\frac{\rho(x)}{|\,f'(x)\,|}. \tag{2.52}$$

The density can remain constant at the origin, provided that the slope $|\,f'(0)\,|$ and $R = \mathrm{e}^{\kappa}$ are equal.

Maps for which the logarithm of the slope at the origin is equal to the escape rate are infinitely steep at the endpoints of the escape interval. Such systems are therefore said to be in the *border state of transient chaos* [400, 541]. Since the density is finite at the origin, the c-measure of the leftmost cylinder at level $n$ is proportional to its length, which in turn is proportional to $\mid f'(0) \mid^{-n}$. Taking into account the compensation factor $R$, we have

$$\mu_1^{(n)} \sim R^n \mid f'(0) \mid^{-n}. \tag{2.53}$$

Since the slope is exactly $R$, $\mu_1^{(n)}$ tends to a constant in the large-$n$ limit. In this case, the natural measure is again concentrated at the origin, and we have $D_1 = 0$. The slope is, however, larger than unity here, and therefore the average Lyapunov exponent is finite: $\lambda_1 = \kappa = \ln R$. The underlying dynamics is intermittent-like, and in spite of the high concentration of trajectories near the origin and the rare bursts, the system is sensitive to initial conditions. The escape process is in fact exponential. This case is called the border state because for the slope $\mid f'(0) \mid$ larger (smaller) than $e^{\kappa}$, transient chaos is hyperbolic (nonhyperbolic). An additional feature of the border state is that, besides the c-measure whose density is finite at the origin and tends to zero at the right end, there exist one or more smooth c-measures that vanish at both ends and have escape rates different from $\ln R$. The asymptotic character of the escape process depends then on the exponent of the initial density $\rho_0$ at the origin [400, 497].

## 2.5 Analytic Example of Transient Chaos in Two Dimensions

A chaotic saddle arising in an invertible two-dimensional map has the appearance of the direct product of two Cantor sets, as shown in Fig. 1.8. A pedagogical dynamical system capable of exhibiting many typical features of a chaotic saddle is the open baker map [753]. The action of the mapping can be described as follows. Take the unit square and cut it by a horizontal line into two pieces of surface area $c_0$ and $1 - c_0$, respectively. The lower rectangle of width $c_0$ is then stretched in the vertical direction by a factor of $a > 1$ and simultaneously compressed in the horizontal direction by a factor $c < 1/2$, while keeping the lower left corner fixed. The upper rectangle is transformed by stretching and compression factors $b > 1$ and $d < 1/2$, respectively, during which its upper right corner is fixed. If stretching is sufficiently strong, i.e., $ac_0 > 1$, $b(1 - c_0) > 1$, the map generates transient chaos. Mathematically, the map can be written as

$$x_{n+1} = cx_n, \quad y_{n+1} = ay_n, \tag{2.54}$$

for $y_n < c_0$, and

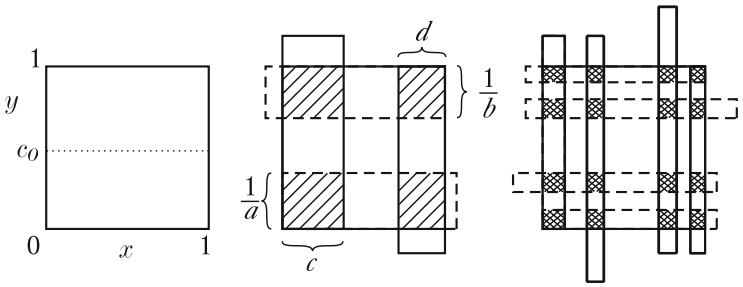


**Fig. 2.14** Open baker map defined on the unit square (the restraining region $\Gamma$). The image (*continuous line*) and preimage (*dashed line*) of the unit square after one and two iterations are shown. Points in the *shaded* and *cross-shaded* regions do not escape the unit square after one and two iterations (forward or backward), respectively

$$x_{n+1} = 1 - d(1 - x_n), \quad y_{n+1} = 1 - b(1 - y_n), \tag{2.55}$$

otherwise. The one and two-step forward and backward images of the unit square are shown in Fig. 2.14. Note that the inverted map is obtained by interchanging the roles of $x$ and $y$ and by replacing $a, b$ by $1/c, 1/d$, and $c, d$ by $1/a, 1/b$, respectively.

Say we distribute $N_0$ initial points on the unit square uniformly. A portion $c_0$ of them falls on the strip elongated by a factor $a$ after the first step. Since only a ratio $1/ac_0$ of the total length overlaps with the unit square, the number of trajectories staying inside the unit square is $N_0/a$. Analogously, from the other strip there are $N_0/b$ surviving trajectories. Altogether, a portion of $(1/a + 1/b)$ of the initial points does not escape the unit square in one time step. The same consideration applies to future iterations as well. As a result, the escape rate is

$$\kappa = -\ln(1/a + 1/b), \tag{2.56}$$

which is the same as that for the tent map (2.28). The positive Lyapunov exponent is also the same as that of the tent map (2.30).

The chaotic saddle of the baker map can be viewed as the direct product of two Cantor sets, and the concept of *partial dimensions* [380, 564] can then be used to characterize the saddle. Specifically, along the $y$-axis the contraction rates defining the Cantor set are $1/a$ and $1/b$, and hence the box-counting dimension along this direction is the solution to the following equation; cf. (1.20):

$$a^{-D_0^{(1)}} + b^{-D_0^{(1)}} = 1, \tag{2.57}$$

where $D_0^{(1)}$ is the *partial box-counting dimension along the unstable direction*. Along the other axis, the contraction rates are $c$ and $d$, and the corresponding dimension is the solution of

$$c^{D_0^{(2)}} + d^{D_0^{(2)}} = 1, \tag{2.58}$$

where $D_0^{(2)}$ is the *partial box-counting dimension along the stable direction*. The box-counting dimension of the chaotic saddle is the sum of the partial dimensions along the stable and the unstable directions:

$$D_0 = D_0^{(1)} + D_0^{(2)}. \tag{2.59}$$

As the concept of c-measure implies (Sect. 1.2.3.2), escape can be compensated by multiplying the number of trajectory points staying *on* the unit square by $\exp(\kappa)$ at each time step. Starting from a uniform distribution on the unit square $\rho_0 \equiv \text{const}$, the probabilities for the two strips in the first step of the open baker map are $\exp(\kappa)/a$ and $\exp(\kappa)/b$. At the $n$th step there are $2^n$ vertical strips of different widths given by $c^m d^{n-m}$, $m = 0, 1, 2, \ldots, n$. The probability of finding trajectory points in strip $j$ of width $c^m d^{n-m}$ is then $\exp(\kappa n) a^{-m} b^{m-n}$. Since the factor appearing after $\exp(\kappa n)$ is just the reciprocal value of the stretching factor (see Sect. 1.2.3.3) $\exp[\Lambda_{1j}(n)]$ for all points in a horizontal strip, we can express the c-measure of strip $j$ at level $n$ by the escape rate and the stretching exponent as

$$\mu_{cj}^{(n)} = \mathrm{e}^{\kappa n} \mathrm{e}^{-\Lambda_{1j}(n)}. \tag{2.60}$$

Qualitatively, this implies that unstable regions with relatively large stretching exponents are less frequently visited. It can also be seen that the limiting c-measure is concentrated on the unstable manifold, whose branches are parallel to the $y$-axis, with constant density.

The natural measure can be obtained in a similar manner. In particular, the common region between the first preimage and image of the square contains points that have not escaped after one forward or one backward iteration. Similarly, the union of the $n$th image and preimage defines trajectories staying inside the square for at least $n$ steps under both the direct and the inverted map, as shown in Fig. 2.14. Points that do not escape thus belong to a double fractal set, the chaotic saddle. Boxes generated by the overlaps of the $n$th images and preimages provide a natural partition of the saddle (the so-called generating partition [220]). To be explicit, we note that the width $\varepsilon_{1i}^{(n)}$ of horizontal strip $i$ is of the type $a^{-m} b^{m-n}$, for $m = 0, 1, \ldots, n$. We can then write

$$\varepsilon_{1i}^{(n)} = \mathrm{e}^{-\Lambda_{1i}(n)}, \tag{2.61}$$

and the width of the vertical strips is

$$\varepsilon_{2j}^{(n)} = \mathrm{e}^{\Lambda_{2j}(n)}, \tag{2.62}$$

where $\Lambda_{2j}$ is the contraction exponent, i.e., the stretching exponent of the inverted map multiplied by $(-1)$. To obtain the natural measure, we note that the smooth density of the c-measure is restricted to boxes of the partition at level $n$, and should be renormalized. Since the weight of a strip has been determined, the renormalization can be done by *keeping the measure of the strip constant*. This means that

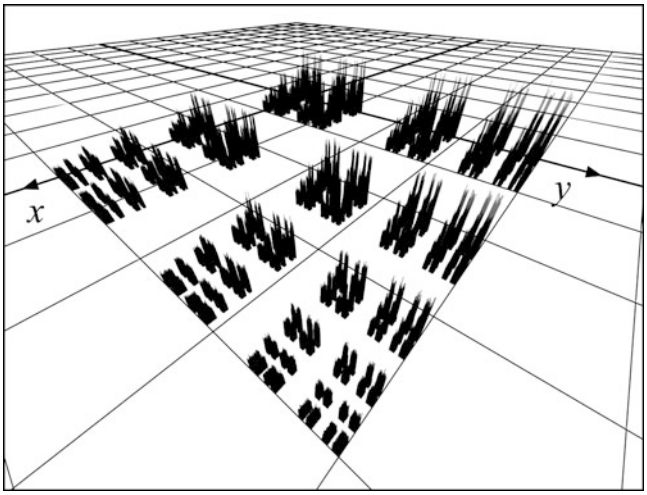


**Fig. 2.15** Natural measure of a chaotic saddle from the baker map. The parameters are a=3, b=2.6, $c = 0.25$, and $d = 0.45$. (Picture by M. Gruiz and Sz. Hadobás.)

(2.60) is valid for the natural measure $\mu_j^{(n)}$ of a full vertical strip as well. For a box of vertical size $\varepsilon_{1i}^{(n)}$ inside a given vertical strip $j$, the natural measure is given by

$$\mu_{ij}^{(n)} = \mu_{cj}^{(n)} e^{\kappa n} \varepsilon_{1i}^{(n)}. \tag{2.63}$$

The exact natural measure can be obtained by taking the $n \to \infty$ limit, as shown by an example in Fig. 2.15. It can be seen that the projections of the natural measure on the $y$- and $x$-axes can be regarded as the measures of the stable and the unstable manifolds, respectively, for $n \gg 1$. There are thus two different fractal distributions embedded in the unit square, characterized by the *partial information dimensions* $D_1^{(1)}$ and $D_1^{(2)}$ along the unstable and the stable directions, respectively. The dimensions are given by

$$D_1^{(1)} = \frac{-a\ln a - b\ln b + (a+b)\ln(a+b)}{a\ln b + b\ln a}, \tag{2.64}$$

$$D_1^{(2)} = \frac{a\ln a + b\ln b - (a+b)\ln(a+b)}{a\ln d + b\ln c}. \tag{2.65}$$

A few remarks are in order.

1. Since the natural measure of a stable strip of order $n$ is also the probability $P(\{S_j\})$ for a binary symbols sequence $\{S_j\}$ of length $n$ to occur ($S_j = 0(1)$ if $y < c_0 (> c_0)$), the metric entropy is the same as in (2.31). The topological entropy is $K_0 = \ln 2$, since all possible binary sequences can occur.

2. The local Jacobian determinant associated with the first iteration of the map is $ac_0c/c_0$ for the lower band and $b(1-c_0)d/(1-c_0)$ for the upper band. The average of the logarithms of these elements is

$$\overline{\ln J} = \frac{b}{a+b}\ln ac + \frac{a}{a+b}\ln bd = \lambda_1 + \lambda_2, \tag{2.66}$$

where $\lambda_2 < 0$ is the negative Lyapunov exponent of the saddle. The dynamics is dissipative if it is phase-space contracting on average, i.e., if $\overline{\ln J} < 0$. The area-preserving case can be obtained if all the local Jacobians are unity, which is the case for $ac = 1 = bd$. This corresponds to an open Hamiltonian system, to be treated in the chapter on chaotic scattering.
3. Note that the dynamical invariants are all independent of the parameter $c_0$. It becomes, however, important in the limit of vanishing escape rates when $c_0 = 1/a$ and $c_0 = 1 - 1/b$ hold, i.e., when both stretching rates are determined by the parameter $c_0$.
4. General hyperbolic chaotic saddles turn out to be smoothly deformed versions of the baker saddle.

## 2.6 General Properties of Chaotic Saddles in Two-Dimensional Maps

### *2.6.1 Natural Measure and c-Measure*

To gain insight into the properties of hyperbolic chaotic saddles arising in two-dimensional maps, we take a restraining region $\Gamma$ of size of the order of unity containing the chaotic saddle, distribute a large number of initial conditions in $\Gamma$, and follow the resulting trajectories in the phase space. The map stretches (contracts) $\Gamma$ along the unstable (stable) direction and bends it so that a part of the image will lie outside $\Gamma$. After $n \gg 1$ iterations the overlap of the image with the original region consists of narrow strips that follow the local unstable directions of the chaotic saddle, which are *unstable strips*, as illustrated in Fig. 2.16. For a hyperbolic chaotic saddle, folds of the unstable manifolds fall outside $\Gamma$, and the corresponding unstable strips will be only slightly bent. The average width $\varepsilon_2^{(n)}$ of an unstable strip is, by definition, proportional to the local contraction factors $\exp[\Lambda_2(n)]$ of points falling, after $n$ steps, in the strip. Due to escape, the majority of the points will be outside $\Gamma$. If after each step the density of points inside is compensated by the factor $\exp(\kappa)$, then a finite limit is found, the density of the conditionally invariant measure.

The equation describing this density can be obtained as follows. The probability of finding points in a small region about $\mathbf{x}$ defines a distribution $\rho_n(\mathbf{x})$ after $n$ steps. Its dynamics is governed by the requirement that the total probability in a

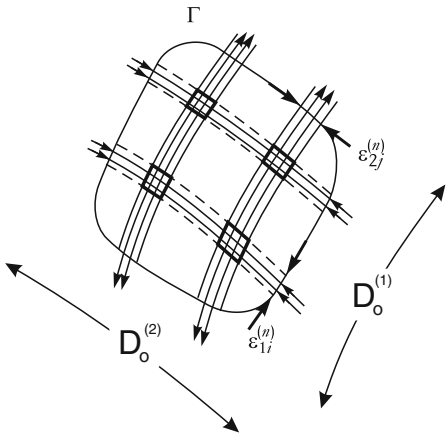


**Fig. 2.16** Schematic diagram of the phase-space partition for a chaotic saddle obtained by taking the $n$th image and preimage of region $\Gamma$ of size unity that covers the saddle. Shown are stable strips (*dashed lines*), unstable strips (*solid lines*), invariant manifolds, and the directions along which the partial dimensions are defined

small region at step $n$ be the same as in the image of that region under the map $\mathbf{f}$, after taking into account the compensation factor [764]:

$$\rho_{n+1}(\mathbf{x}') = \mathrm{e}^{\kappa} \frac{\rho_n(\mathbf{x})}{|J(\mathbf{x})|}\Big|_{\mathbf{x}\in\mathbf{f}^{-1}(\mathbf{x}')}, \tag{2.67}$$

where $J(\mathbf{x})$ is the Jacobian determinant at the point $\mathbf{x}$. This is the Frobenius–Perron equation for open invertible two-dimensional maps. Similar to the one-dimensional case (cf. (2.2)), for any smooth initial density $\rho_0(\mathbf{x})$ the density $\rho_n(\mathbf{x})$ converges for $n \to \infty$ to a limit density $\rho(\mathbf{x})$, the density of the c-measure. The resulting c-measure has a smooth, but *not necessarily constant*, density along the unstable manifold. The fact that the largest eigenvalue $\exp(-\kappa)$ of the Frobenius–Perron operator is less than unity ensures again the exponential decay.

It is worth pointing out an analogy with the concept of *almost invariant sets* introduced by Dellnitz, Froyland, and coworkers [174,250]. Such sets are regions in the phase space from which a point escapes with a small probability in a period of time. Chaotic saddles and their manifolds are invariant sets. A neighborhood of the unstable manifold, e.g., can, however, be considered to be almost invariant, provided that the escape rate is low. The regions of slow escape determine, in general, a pattern related to the Frobenius–Perron (or transfer) operator defined by (2.67). The eigenfunction belonging to the largest eigenvalue below unity provides the backbone of this pattern. This largest eigenvalue is $\exp(-\kappa)$ in our case, and the eigenfunction $\rho(\mathbf{x})$ concentrates on the pattern of the unstable manifold, as Fig. 1.11 illustrates.

We turn now to the determination of the natural measure. Without compensating for the escaping, the measure of an unstable strip is proportional to the area of its $n$th preimage. The $n$th preimage of $\Gamma$ consists of strips that are parallel to the local stable directions of the chaotic saddle. The average width $\varepsilon_{1,j}^{(n)}$ of a stable strip, as shown in Fig. 2.16, is proportional to the contraction factor of the inverted map, i.e., to the reciprocal of the stretching factor of the forward map: $\varepsilon_{1,j}^{(n)} \sim \exp[-\Lambda_{1,j}(n)]$, where $\Lambda_{1,j}(n)/n$ is the positive Lyapunov exponent of points inside the strip.

The $n$th image of such a strip will then have side lengths of order unity and of order $\exp[\Lambda_{2,i}(n)]$ along the unstable and the stable directions, respectively. As a result, a stable strip is nothing but the $n$th preimage of an unstable one. The measure of an unstable strip $j$ without compensating for the escape is thus proportional to $\varepsilon_{1,j}^{(n)}$, the width of the $n$th preimage of the unstable strip. Taking into account the compensation, we find that the c-measure contained in the unstable strip $j$ is given by

$$\mu_{\mathrm{c}j}^{(n)} \approx \mathrm{e}^{\kappa n}\varepsilon_{1j}^{(n)} \sim \mathrm{e}^{\kappa n}\mathrm{e}^{-\Lambda_{1j}(n)}. \tag{2.68}$$

The natural measure is obtained by taking the overlap between the $n$th image and preimage of the region $\Gamma$, which provides, for large $n$, a partition of the phase space and an accurate coverage of the chaotic saddle [45, 220]. The natural measure of a box in the partition can be obtained by redistributing the c-measures of unstable strips according to the length scales $\varepsilon_1^{(n)}$. In particular, in unstable strip $j$, the natural measure of box $i$ of length $\varepsilon_{1i}$ can be expressed as

$$\mu_{ij}^{(n)} \approx \mu_{\mathrm{c}j}^{(n)}\mathrm{e}^{\kappa n}\varepsilon_{1i}^{(n)}. \tag{2.69}$$

It should be emphasized that $\mu_{\mathrm{c}j}^{(n)}$ as given by (2.68) is in fact the natural measure $\mu$ of strip $j$: $\mu_j^{(n)} = \mu_{\mathrm{c}j}^{(n)}$. Formally, this follows from $\sum \varepsilon_{1i}^{(n)} \approx \exp(-\kappa n)$, which holds because escape takes place along the unstable direction only.

The natural measure of stable strips can be obtained in a similar manner. By summing (2.69) over $j$ and utilizing $\sum_j \mu_{\mathrm{c}j}^{(n)} = 1$, one finds the natural measure of stable strip $i$ to be

$$\mu_i^{(n)} \approx \mathrm{e}^{\kappa n}\varepsilon_{1i}^{(n)}, \tag{2.70}$$

which is the same as for its $n$th image, an unstable strip. This reflects the fact that the natural measure is preserved under the map.

Qualitatively speaking, maps generating hyperbolic chaotic saddles can be locally decomposed into baker's transformations. The actual form of the local map can change with the position only smoothly. This is the reason that the general expressions for the natural measures are similar to those obtained for the chaotic saddle of the baker's map.

### 2.6.2 *Entropy and Dimension Formulas*

The stretching factor for points in the stable strip $i$ is given by $\exp[\Lambda_{1i}(n)] \sim 1/\varepsilon_{1i}^{(n)}$. The natural measure of this strip is given by (2.70). Replacing $P_i(\varepsilon)$ in (1.18) by $\mu_i^{(n)}$, we obtain the average Lyapunov exponent $\lambda_1 > 0$ as

$$\lambda_1 = -\frac{1}{n}\sum_i \varepsilon_{1i}^{(n)}\mathrm{e}^{\kappa n}\ln\varepsilon_{1i}^{(n)}, \tag{2.71}$$

where the summation is over all stable strips. In an analogous way, the contracting average Lyapunov exponent $\lambda_2 < 0$ is obtained as

$$\lambda_2 = \frac{1}{n} \sum_j \varepsilon_{1j}^{(n)} \mathrm{e}^{\kappa n} \ln \varepsilon_{2j}^{(n)}. \tag{2.72}$$

The negative Lyapunov exponent ensures that trajectories from random initial conditions approach the chaotic saddle. In fact, the time needed for the survival probability to begin to decay exponentially (the value of $n^*$ in (1.8)) is approximately $1/\mid \lambda_2 \mid$.

The metric entropy follows from (1.24) by observing that the measure $\mu_i^{(n)}$ of a stable strip is simultaneously a path probability for all points within that strip, and can be written as

$$K_1 = -\frac{1}{n} \sum_i \varepsilon_{1i}^{(n)} \mathrm{e}^{\kappa n} \left( \kappa n + \ln \varepsilon_{1i}^{(n)} \right). \tag{2.73}$$

Comparing (2.71) and (2.73), we obtain again the relation

$$K_1 = \lambda_1 - \kappa, \tag{2.74}$$

which implies that the dynamics along the unstable manifold of an invertible two-dimensional map is indeed similar to that in a one-dimensional map. This can also be seen by examining the partial information dimension along the unstable manifold (cf. Fig. 2.16). In particular, from (1.22), we have

$$D_1^{(1)} = \frac{\sum_i \mu_i^{(n)} \ln \mu_i^{(n)}}{\sum_i \mu_i^{(n)} \ln \varepsilon_{1i}^{(n)}}, \tag{2.75}$$

which leads to

$$D_1^{(1)} = 1 - \frac{\kappa}{\lambda_1}. \tag{2.76}$$

The partial information dimension along the stable manifold is given by

$$D_1^{(2)} = \frac{\sum_j \mu_j^{(n)} \ln \mu_j^{(n)}}{\sum_j \mu_j^{(n)} \ln \varepsilon_{2j}^{(n)}}. \tag{2.77}$$

Since the denominator is $n$ times the negative Lyapunov exponent $\lambda_2$, we obtain

$$D_1^{(2)} = \frac{\lambda_1 - \kappa}{|\lambda_2|} = \frac{\lambda_1}{|\lambda_2|} D_1^{(1)}. \tag{2.78}$$

Relations (2.76) and (2.78) are the dimension formulas, also called the Kantz–Grassberger relations [380], for chaotic saddles arising from two-dimensional maps.

The total information dimension is the sum of the partial dimensions:

$$D_1 = K_1 \left( \frac{1}{\lambda_1} + \frac{1}{|\lambda_2|} \right). \tag{2.79}$$

In the limit of chaotic attractors where $\kappa = 0$, $K_1 = \lambda_1$, (2.79) reduces to the Kaplan–Yorke formula [386] for two-dimensional maps.

One can see that the metric entropy is the product of the magnitude of the Lyapunov exponent and the partial information dimension along either the stable or the unstable direction [564, 773]:

$$K_1 = \lambda_1 D_1^{(1)} = |\lambda_2| D_1^{(2)}. \tag{2.80}$$

For a two-dimensional map, there is only one positive Lyapunov exponent. The topological entropy $K_0$ is then determined by the exponent and its cumulants, as for a one-dimensional map. Formula (2.22) thus remains valid. Similarly, the formula for the escape rate can be generalized by replacing $D_0$ in (2.21) by the partial box-counting dimension along the unstable direction. We have

$$\kappa = \left(1 - D_0^{(1)}\right) \lambda_1 + \frac{1}{2} \left(1 - D_0^{(1)}\right)^2 Q_2 + \cdots. \tag{2.81}$$

The box-counting and information dimensions $D_{\mathrm{s},i}$ and $D_{\mathrm{u},i}$ ($i = 0, 1$) of the stable and unstable manifolds are related to the partial dimensions as

$$D_{\mathrm{s},i} = 1 + D_i^{(1)} \quad \text{and} \quad D_{\mathrm{u},i} = 1 + D_i^{(2)}, \tag{2.82}$$

since the manifolds are locally smooth (one-dimensional) curves. The dimension of the full chaotic saddle can also be expressed through the manifold dimensions as

$$D_i = D_{\mathrm{s},i} + D_{\mathrm{u},i} - 2. \tag{2.83}$$

Note that in the dimension and entropy formalism discussed, the roles of the sets $\{\varepsilon_1^{(n)}\}$ and $\{\varepsilon_2^{(n)}\}$ are not equal, since the natural measure is connected with one of them only; cf. (2.69). Interchanging $\{\varepsilon_1^{(n)}\}$ and $\{\varepsilon_2^{(n)}\}$ in fact yields dimension and entropy formulas associated with the natural distribution of the inverted map.

### *2.6.3 Information-Theoretic Arguments*

The dimension and entropy formulas treated in Sect. 2.6.2 play a central role in the study of transient chaos, which can in fact be derived using an information-theoretic approach. In particular, the evolution of a chaotic system is unpredictable in long terms. In communication, it was realized by Shannon in 1948 that a sequence of

events conveys information if the events are not fully predictable [71, 283, 708]. The fundamental unpredictability of chaos thus implies that chaotic systems can be regarded as sources of information. We have seen that the metric entropy $K_1$ is the rate at which information flows toward the significant digits, with the mean flow velocity given by the average Lyapunov exponent $\lambda_1$ (Sect. 1.2.3.3). This observation led Kantz and Grassberger to argue [380] that the partial information dimension $D_1^{(1)}$ is nothing but the density of information per digit on average. As a result, (2.80) expresses that the flow rate equals the product of velocity and density. The same amount of information flow is expected along the stable direction.

Escape can take place only along the unstable manifold. If its partial information dimension were unity, no exponential decay would occur along this direction. The difference $(1-D_1^{(1)})$ is thus proportional to the escape rate. Since the velocity of the information flow is $\lambda_1$, we have $\kappa = \lambda_1(1-D_1^{(1)})$, which is equivalent to (2.76).

Similarly, the relation $\lambda_1 = K_1 + \kappa$ (see (2.74)) can be viewed as a consequence of the fact that only a portion of the mean velocity of the information flow contributes to information generation, since only the fraction $K_1/\lambda_1$ of the mean velocity contributes to the unpredictability associated with the dynamics on the nonattracting set. The remaining fraction $\kappa/\lambda_1$ is in fact associated with the process of escape.

Although the information-theoretic arguments are heuristic, assumptions such as hyperbolicity and invertibility of the dynamics are not necessary. Thus the basic formulas as given by (2.74), (2.76), (2.78), and (2.80) are expected to be valid for *nonhyperbolic* dynamical systems in general.

### 2.6.4 Organization About Unstable Periodic Orbits

Unstable periodic orbits are the fundamental building blocks of any chaotic set, attracting or nonattracting. A chaotic set is densely covered by an infinite number of unstable periodic orbits, and hence they determine the natural distribution on the set. Chaotic motion can be interpreted as a *random walk among periodic orbits*, or cycles. In particular, when a chaotic trajectory approaches a specific periodic orbit, in a short time interval the behavior of the trajectory is approximately periodic. Since the orbit is unstable, the trajectory will leave the orbit but then approach a different periodic orbit, and so on. This suggests that the invariant characteristics of the chaotic set can be expressed in terms of the properties of the various unstable periodic orbits. Indeed, natural measures associated with chaotic attractors can be characterized by unstable periodic orbits [63, 297, 435, 459], and the same can be done for chaotic saddles [151, 187, 765]. Chaotic saddles are the *closures* of all the embedded unstable periodic orbits.

The stability of an unstable periodic orbit of period $n$ is determined by its cycle eigenvalues, which for a map system are the eigenvalues of the linearized $n$th iterated map evaluated at the orbit. Chaos can thus be characterized by means of the cycle eigenvalues, provided that sufficiently many periodic orbits can be determined and analyzed.

For a one-dimensional map of the type in Fig. 2.1, the various cylinder lengths can be expressed by the cycle eigenvalues. The fixed points of the $n$th iterated map, all period-$n$ points, are the intersecting points of the diagonal line with the graph of $f^n$. It can be seen from Fig. 2.3 that each cylinder of level $n$ contains one $n$-cycle point. The slope of $f^n$ at a cycle point is approximately the same for any point of the cylinder containing this periodic orbit. As a result, we have $\varepsilon_i^{(n)} \sim 1/\mid f^{n\prime}(x_i^*)\mid$, where $x_i^*$ is the $n$-cycle point belonging to cylinder $i$. We see that the length scales of the generating partition for the natural distribution are determined by the stabilities of various periodic orbits embedded in the underlying chaotic set.

Now consider a two-dimensional map. To be concrete, we can take unstable strip $j$ and determine its $n$th preimage. The overlap between them defines points that return approximately to their initial positions after $n$ steps, and the overlap thus contains a hyperbolic $n$-cycle point. The magnitudes of the cycle eigenvalues can be written as $\exp(\lambda_{lj}^* n)$ $(l = 1,2)$, where $\lambda_{1j}^* > 0$ and $\lambda_{2j}^* < 0$ are the local Lyapunov exponents of the periodic orbit. The contracting eigenvalue $\lambda_{2j}^*$ of the period-$n$ point in unstable strip $j$ defines the width of this strip:

$$\varepsilon_{2j}^{(n)} \approx \mathrm{e}^{\lambda_{2j}^* n}. \tag{2.84}$$

Similarly, the width of the $n$th preimage strip is the reciprocal value of $\exp(\lambda_{1j}^* n)$:

$$\varepsilon_{1j}^{(n)} \approx \mathrm{e}^{-\lambda_{1j}^* n}. \tag{2.85}$$

With this expression, the measure (2.68) of the unstable strip can be expressed by the eigenvalue of the period-$n$ orbit in this strip as

$$\mu_j^{(n)} \approx \frac{\mathrm{e}^{\kappa n}}{\mathrm{e}^{\lambda_{1j}^* n}}. \tag{2.86}$$

This relation has been shown to hold for nonhyperbolic chaotic saddles in dissipative dynamical systems as well [186].

We see that strips with more unstable orbits are less probable. Taking into account the normalization condition $\sum_j \mu_j^{(n)} = 1$, where the summation is taken over all the strips at level $n$, i.e., all the periodic orbits of length $n$, we see that the sum of the reciprocals of the expanding eigenvalues is not of order unity (as it would be for attractors), but tends toward zero for large $n$. The escape rate can be expressed in terms of the eigenvalues of all period-$n$ orbits as

$$\mathrm{e}^{-\kappa n} = \sum_j \frac{1}{\mathrm{e}^{\lambda_{1j}^* n}} \quad \text{for } n \gg 1, \tag{2.87}$$

where the summation is taken over all period-$n$ points on the chaotic saddle. The average Lyapunov exponent can be expressed as a similar sum, from (2.71),

$$\lambda_1 = \sum_j \lambda_{1j}^* \frac{\mathrm{e}^{\kappa n}}{\mathrm{e}^{\lambda_{1j}^* n}} \quad \text{for } n \gg 1. \tag{2.88}$$

The metric entropy (2.73) then appears as the average of $\lambda_{1j}^* - \kappa$, from which (2.74) follows.

The fractal properties of the natural measure can also be related to the cycle eigenvalues. To see this, consider a small box of dimensions $l_1$ and $l_2$ along the unstable and stable directions, respectively, about a point of the $i$th cycle of length $n$. Since the c-measure is smooth along the unstable direction, the c-measure of the box scales with $l_1$ and $l_2$ as

$$\mu_c(l_1, l_2) \sim l_1 l_2^{\alpha_{2i}}, \tag{2.89}$$

where $\alpha_{2i} < 1$ is a nontrivial exponent, the local *crowding index* characterizing the local fractal structure along the stable direction. After $n$ iterations, the box is stretched (compressed) by factors of $\exp(\lambda_{1i}^* n)$ and $\exp(\lambda_{2i}^* n)$ along the unstable and stable manifolds, respectively, where $\lambda_{1i}^*$ and $\lambda_{2i}^*$ are the local Lyapunov exponents of the whole cycle. The side lengths of the $n$-fold image of the box are thus $l_1 \exp(\lambda_{1i}^* n)$ and $l_2 \exp(\lambda_{2i}^* n)$. Due to escape, the c-measures of the original box and of its images are different. A stationary distribution can be obtained when the escape is compensated for by the factor $\exp(\kappa n)$:

$$e^{\kappa n} \mu_c(l_1, l_2) = \mu_c(l_1 e^{\lambda_{1i}^* n}, l_2 e^{\lambda_{2i}^* n}). \tag{2.90}$$

Using the scaling from (2.89), we obtain

$$\lambda_{1i}^* - \kappa + \lambda_{2i}^* \alpha_{2i} = 0. \tag{2.91}$$

The natural measure $\mu$ of the same box scales with $l_1$ and $l_2$ as

$$\mu(l_1, l_2) \sim {l_1}^{\alpha_{1i}} {l_2}^{\alpha_{2i}}, \tag{2.92}$$

where $\alpha_{1i} < 1$ is the crowding index along the unstable direction, and $\alpha_2$ is the same for both the natural and the c-measures. Preservation of the natural measure requires

$$\lambda_{1i}^* \alpha_{1i} + \lambda_{2i}^* \alpha_{2i} = 0. \tag{2.93}$$

Equations (2.91) and (2.93) indicate that the set of local crowding indices are uniquely determined by the cycle eigenvalues, from which $\alpha_1$ can be obtained as

$$\alpha_{1i} = 1 - \frac{\kappa}{\lambda_{1i}^*}. \tag{2.94}$$

Since the crowding indices are a kind of local partial information dimensions, (2.94) and (2.93) are the local analogues of the dimension formulas (2.76) and (2.78), respectively.

## 2.7 Leaked Dynamical Systems and Poincaré Recurrences

### *2.7.1 Chaotic Saddles Associated with Leaked Systems*

When a closed chaotic system is probed experimentally, the window through which observations are made can induce "leaking" of trajectories. Escape can thus occur, leading to transient chaos. The invariant sets of a leaked dynamical system are *subsets* of those in the corresponding closed system. Cutting a hole in a closed system to generate transient chaos was first suggested by Pianigiani and Yorke [596], and has since been studied in several contexts (see, e.g., [354, 572, 573], and [19] for a recent review). Since leaked chaotic systems provide a tool for a better understanding of the closed dynamics, leaking can be regarded as a type of chaotic spectroscopy [202, 203], or a way of "peeping at chaos" [105, 179].

To define leaking, we take a closed system described by a map $\mathbf{f}_{\text{closed}}(\mathbf{x})$ and choose a subset $I$ of the phase space $\Omega$, which is the leaking region, or the leak for short. A trajectory is regarded as having escaped the system after entering the region $I$. The leaked dynamics can thus be described by the following map:

$$\mathbf{x}_{n+1} = \mathbf{f}(\mathbf{x}_n) = \begin{cases} \mathbf{f}_{\text{closed}}(\mathbf{x}_n) & \text{if } \mathbf{x}_n \notin I, \\ \text{escape} & \text{if } \mathbf{x}_n \in I. \end{cases} \tag{2.95}$$

Since escape is considered to occur one step *after* entering $I$, the map $\mathbf{f}$ is defined in $I$. There is a chaotic saddle in the leaked system, which is the set of points that do not escape the *complement* of the leaking region $I$ for both forward and backward iterations and is responsible for the exponential decay of the survival probability of trajectories in the system with some escape rate $\kappa$. The saddle is a subset of the original chaotic set in the corresponding closed system. An example from the Hénon map [325] is shown in Figs. 2.17a, b, where (a) shows a chaotic attractor and (b) displays the resulting chaotic saddle when the leaking region is a disk in the phase space. The chaotic saddle resembles mostly that of the Hénon map in the transiently chaotic regime (Fig. 1.8) except that the unstable manifold of this saddle is no longer a continuous curve as in Fig. 1.7. In general, the unstable manifold of a leaked dynamical system consists of disjoint pieces separated by the leaking region and its images.

As another example, consider the single-scale, area-preserving baker map. The phase space $\Omega$ is the unit square. Without any leak, a typical trajectory originated from a random initial condition visits the entire square with uniform probability. The natural measure $\mu$ is thus the Lebesgue measure. Suppose there is a leak in the system defined as a band extending over the full phase, where the center of the leaking region $I$ is chosen to be the center of the unit square. The area $\mu(I)$ of the leak and the angle $\theta$ of the band relative to the $y$-axis are the two parameters that can be changed systematically. Invariant sets of the leaked baker map for leaks of the same area but with opposite tilt angles are shown in Fig. 2.18. The escape rates for these sets are different: $\kappa(25^\circ) = 0.11$ and $\kappa(-25^\circ) = 0.09$. For better visibility,

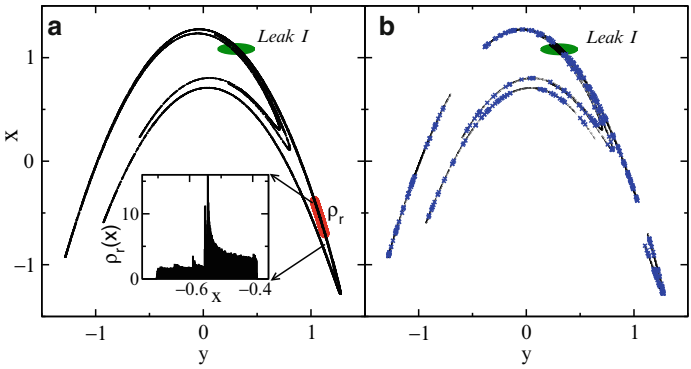


**Fig. 2.17** For the Hénon map $x_{n+1} = 1 - 1.4x_n^2 + y_n$ and $y_{n+1} = 0.3x_n$, (**a**) chaotic attractor (*thin line*), the leaking region $I$ and its first image $\mathbf{f}(I)$ (*gray regions*). The inset shows the projection $\rho_r(x)$ of the first image of the natural measure of the attractor in the leaking region on the $x$-axis. (**b**) Chaotic saddle (*crosses*) and its unstable manifold (*thin line*) of the corresponding leaked system. These invariant sets are generated using the sprinkler method (Sect. 1.2.2.3) with $n_0 = 40$

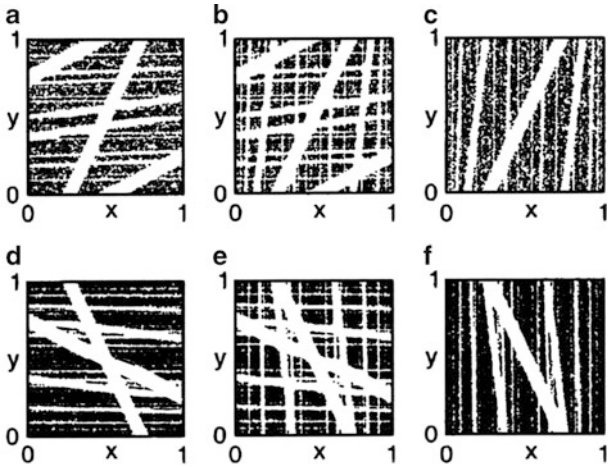


**Fig. 2.18** For the baker map given by $(x_{n+1}, y_{n+1}) = (x_n/2, 2y_n)$ for $y_n \leq 1/2$ and $(x_{n+1}, y_{n+1}) = (1 + 1/2(x_n - 1), 1 + 2(y_n - 1))$ for $y_n > 1/2$ with a tilted leak of area $\mu(I) = 0.1$ at the angle $\theta = 25^\circ$ and $\theta = -25^\circ$, respectively, the stable manifold (**a**), (**d**), the chaotic saddle (**b**), (**e**), and the unstable manifold (**c**), (**f**). The difference in the contrast of the pictures is due to the difference in the escape rates [688] (Copyright 2002, the American Physical Society)

points of the invariant manifolds are not displayed within the leak. The leak is thus visible in Fig. 2.18 as a white band crossing the center of the square. There are in fact many more white bands. In particular, in the plot of the stable (unstable) manifold, these are the preimages (images) of the leak, and in the plot of the chaotic saddle

both the preimages and the images are present. In spite of the uniform density, the action of the baker map is asymmetric. The preimages of the left- and right-tilted bands are quite different. As a result, the first preimage of the 25° leak does not overlap with the leak, but there is an overlap in the other case. Thus, the total area of the leak and its first preimage is larger for the positive-angle case than that for the negative-angle case. The asymmetry persists in subsequent iterations, leading to different escape rates.

Figure 2.19 provides an overview of the chaotic saddles for the same leak area $\mu(I)$ but at a different set of angles $\theta$. The textures at angles of opposite signs are quite different. The dependence of the escape rate on both parameters is summarized in Fig. 2.20. The escape rates associated with narrow leaks are nearly orientation-independent. In addition, the values of $\kappa$ are close to the total area of the leak. Orientation dependence becomes significant for $\mu(I) > 0.05$, and the amount of fluctuations about the mean increases as the area is increased. In all cases, the intuitive estimate obtained from the assumption that $\exp(-\kappa)$ equals $1 - \mu(I)$,

$$\kappa(I) \approx -\ln[1 - \mu(I)], \tag{2.96}$$

is below the average escape rate over all the angles, but as Fig. 2.20 indicates, it provides a good approximation for small areas.

Since all periodic orbits in the used baker map have the same Lyapunov exponent, the average positive Lyapunov exponent of the chaotic saddle is $\lambda_1 = \ln 2$. The topological entropy is equal to the metric entropy. From (2.74), we obtain

$$K_0 = \lambda_1 - \kappa = \ln 2 - \kappa. \tag{2.97}$$

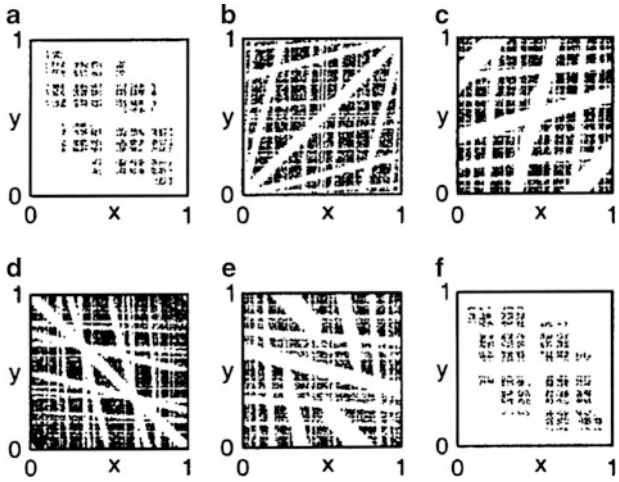


**Fig. 2.19** Chaotic saddles of the leaked baker map ($\mu(I) = 0.1$) at leak angles $\theta = 0°$ (**a**), 45° (**b**), and 75° (**c**), and $\theta = -45°$ (**d**), $\theta = -75°$ (**e**), and $\theta = \pm 90°$ (**f**) [688] (Copyright 2002, the American Physical Society)

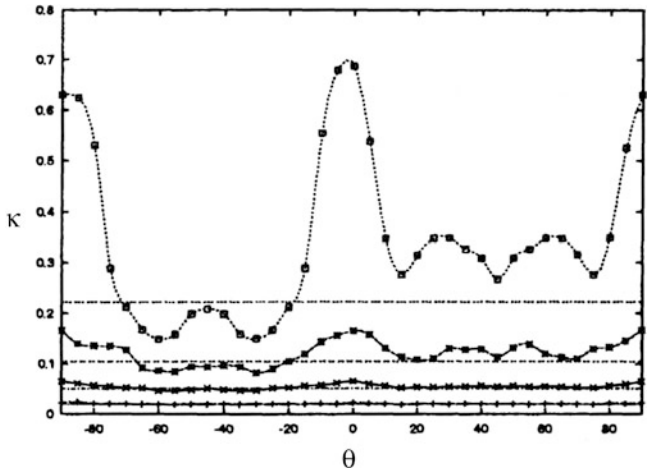


**Fig. 2.20** Dependence of the escape rate on the tilt angle for different leak areas $\mu(I) = 0.02$ (*plus*), 0.05 (*crosses*), 0.1(*asterisk*), and 0.2 (*squares*). *Horizontal lines* correspond to the values $-\ln(1-\mu(I))$ [688] (Copyright 2002, the American Physical Society)

The deviation of $K_0$ from $\ln 2$ indicates that not all possible sequences in the symbolic encoding are allowed to exist. The relatively large difference in the escape rates for different leaks thus reflects the difference in the topological entropies and in the rules underlying the symbolic dynamics.

From (1.14), it can be seen that the escape rate can be expressed in terms of the c-measure of the set of points that do not escape within one iteration. This set is $\Omega \setminus I$, where $\Omega$ is the phase space of the closed system. Since $\mu_c(\Omega \setminus I) = \mu_c(\Omega) - \mu_c(I)$ and the c-measure of the full phase space is normalized to be unity, we have $\mu_c(\Omega \setminus I) = 1 - \mu_c(I)$. This leads to an exact relation for the escape rate of the leaked system:

$$\kappa(I) = -\ln[1 - \mu_c(I)]. \tag{2.98}$$

That is, the escape rate is determined by the c-measure of the leak. The strong dependence of the escape rate on the orientation in Fig. 2.20 reflects that the c-measure can be drastically different even if the natural measure of the leak is kept constant [102]. The strong dependence of the c-measure on the orientation is also a consequence of the different kinds of grammatical rules in the symbolic dynamics due to the different overlaps of the preimages.

In the limit where the leak area becomes infinitesimally small, the escape rate approaches zero and the c-measure tends thus to the Lebesgue measure [5, 167]. It is only in the limit of $\mu_c(I) \to \mu(I) \to 0$ that the estimate (2.96) coincides with the exact result in (2.98). In this case, we have $\kappa = \mu(I)$, so that both the survival probability and the escape time distribution decay with time as

$$P(n) \sim p(n) \sim \mathrm{e}^{-\mu(I)n}. \tag{2.99}$$

The average lifetime is then

$$\tau = \frac{1}{\mu(I)} \quad \text{for } \mu_c(I),\ \mu(I) \to 0. \tag{2.100}$$

For larger leaks, the escape rate is given by (2.98), and no general formula can be obtained for the average lifetime, since this quantity depends also on the initial conditions.

Relation (2.99) has been used in several problems in dynamical systems ranging from fractal exit boundaries [72,538,623,668] and the control of chaos [101,571] to leaked billiards [43,179–181,475,476,539] and intermittency [836]. An interesting application is the reinterpretation of Sabine's law, a central object of architectural acoustics. The law says that the residual sound intensity in a room decays exponentially with time, and the decay rate is independent of the location of the source and the details of the room, provided that the room's shape is sufficiently irregular [532]. The duration to decay below the audible intensity is called the reverberation time. What is escaping here is not trajectories, but the energy of the sound waves, and the leak is the union of all energy-absorbing surfaces. In the language of the theory of dynamical systems, the reverberation time is the reciprocal of the escape rate, which is proportional to the natural measure of the leak, provided that the escape rate is small. Sabine's law, dating back to 1898, appears thus to be the first application of transient chaos in the history of science.

Finally, we mention the general case of more than one separated leak. For instance, with two leaks $I_1$ and $I_2$, the escape rate is in general different from the sum of the single leaked cases:

$$\kappa(I_1 + I_2) \neq \kappa(I_1) + \kappa(I_2). \tag{2.101}$$

The difference is due to the overlap of the preimages of the two leaks [101, 574], which has been established rigorously by Bunimovich and Dettmann [105]. In the limit of small leaks, the difference can be expressed in terms of the correlation function of the temporal dynamics.

### *2.7.2 Poincaré Recurrences*

Poincaré recurrence, the return of trajectories to a specific region in the phase space, have played an important role in the study of closed dynamical systems because they constitute the foundation of the kinetic description of nonequilibrium processes [201, 851, 852]. In a macroscopic system the average recurrence time is typically large, but it tends to be smaller in low-dimensional systems. Poincaré recurrences have also been shown to provide useful insights into the dynamics of chaotic systems [16, 38, 136, 853]. An important quantity is the distribution $p_r(k)$ of the first Poincaré recurrence times $k$ to a preselected region $I$ in the phase space.

As originally proposed by Chirikov and Shepelyansky [136], the *recurrence time distribution* $p_{\rm r}(k)$ is a useful quantity in the analysis of dynamics in the full phase space. The Poincaré recurrence theorem ensures that for almost all initial conditions $\mathbf{x}_0$ in $I$, there are infinitely many time instants $n = n_1, n_2, \ldots$ such that $\mathbf{f}^n(\mathbf{x}_0) \in I$. The first recurrence times are defined as $k = n_i - n_{i-1}$ for $i = 0, 1, \ldots$, and $k = 1$ if the point remains in $I$. The recurrence time distribution $p_{\rm r}(k)$, $k \geq 1$, is the probability of finding recurrence time $k$ from an infinitely long trajectory. Due to the ergodicity of the natural measure of the closed system, the specific choice of the initial point $\mathbf{x}_0 \in I$ is irrelevant for $p_{\rm r}(k)$. In the original setting, the recurrence region $I$ is taken to be arbitrarily small, but in practical applications the size of $I$ is finite, which we will assume in what follows.

For a generic chaotic system, the distribution $p_{\rm r}(k)$ of recurrence times is found for any leak size to have the form [16]

$$p_{\rm r}(k) \approx \begin{cases} \text{fluctuations} & \text{for } 1 < k < k_{\rm r}^*, \\ g_r \mathrm{e}^{-\gamma k} & \text{for } k \geq k_{\rm r}^*. \end{cases} \tag{2.102}$$

The asymptotic behavior is an exponential decay with a decay rate $\gamma$. The short-time nonexponential behavior occurring before the exponential decay depends on the choice of the recurrence region $I$. A consequence of ergodicity of the natural measure is Kac's lemma [372], which states that the mean recurrence time $\tau_{\rm r} \equiv \sum_k k p_{\rm r}(k)$ is the reciprocal of the *natural measure* of the recurrence region:

$$\tau_{\rm r} = \frac{1}{\mu(I)}. \tag{2.103}$$

Equation (2.103) is valid for any size of the recurrence region $I$. The decay rate $\gamma$, however, cannot be given in terms of the natural measure.

The recurrence problem can be better understood in the context of leaked dynamical systems. In particular, one can choose the *recurrence region to be the leak* and examine the interplay between the recurrence and escape times [18]. In this setting, trajectories contributing to the asymptotic decay of Poincaré recurrences must, after exiting the recurrence region $I$, fall into the neighborhood of the stable manifold of the chaotic saddle of the leaked system. The long-time dynamics preceding the first arrival back to the recurrence region is governed by the same saddle underlying the escape process in the leaked system. As a result, the relaxation rate of the recurrence statistics coincides with the decay rate of the escape statistics:

$$\gamma = \kappa. \tag{2.104}$$

The slopes of the recurrence time distribution $\ln p_{\rm r}(n)$ and of the escape time distribution $\ln p(n)$ are thus identical, as illustrated in Fig. 2.21 for the standard Hénon attractor with the recurrence/leak region $I$ chosen as in Fig. 2.17. Equation (2.104) implies that for any Poincaré recurrence problem, there exists a chaotic saddle in the corresponding leaked system and the relaxation rate $\gamma$ is given by the escape rate from the saddle. It is remarkable that in view of (2.98), the relaxation

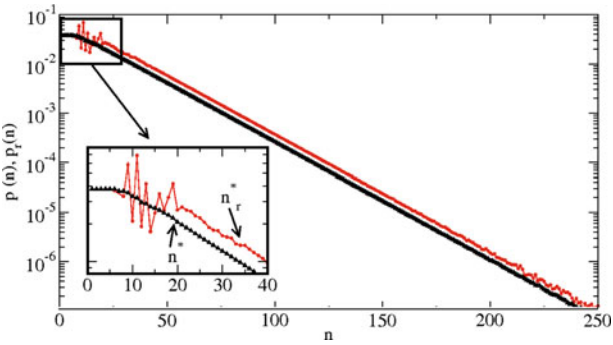


**Fig. 2.21** For the Hénon map with leaking region $I$ chosen as in Fig. 2.17, (**a**) distributions of recurrence time $p_{\rm r}(n)$ and of escape time $p(n)$. To generate $p_{\rm r}(n)$, a trajectory of length $10^{11}$ originated from the center point of the recurrence region is used. The initial conditions for the escape-time distribution $p(n)$ of the leaked system are chosen according to the natural distribution of the Hénon attractor. Short-time behaviors of the distributions are shown in the *inset*; $\gamma = \kappa = 0.055$. The value $n^*$ (respectively $n_r^*$) indicates the time after which the decay of $p(n)$ (respectively $p_{\rm r}(n)$) is exponential with good accuracy [18] (Copyright 2008, the American Physical Society)

rate of the Poincaré recurrences of a closed system is given by the c-measure (rather than by the natural measure) of the recurrence region when viewed as a leaked system.

Despite exhibiting the same exponential decay, the distributions $p_{\rm r}(n)$ and $p(n)$ are different for typical initial distributions $\rho_0$. There is, however, a special initial condition $\rho_0 = \rho_{\rm r}$ for the leaked problem for which the escape statistics are fully equivalent to the recurrence statistics. Consider the distribution obtained as the first iterate of the points $\mathbf{x} \in I$ distributed according to the natural density $\rho_\mu$ of the closed system within the leak. For invertible maps $\mathbf{f}$ with constant Jacobian, this can be written as

$$\rho_r(\mathbf{x}) = \begin{cases} \rho_\mu[\mathbf{f}^{-1}(\mathbf{x})]/\mu(I) & \text{if } \mathbf{x} \in \mathbf{f}(I), \\ 0 & \text{otherwise}, \end{cases} \tag{2.105}$$

where a proper normalization factor has been included in the denominator. The inset of Fig. 2.17a shows an example: the projection of the distribution on one of the dynamical variables of the Hénon map. Due to ergodicity, points of a long trajectory generating the recurrence-time distribution, one iteration after returning to $I$, are distributed precisely according to $\rho_{\rm r}$. As illustrated in Fig. 2.22, due to the definition (2.95), according to which escape takes place one step after entering the leak, all escape times $n$ correspond to the recurrence time $k = n$. Accordingly, we have

$$p_{\rm r}(n) = p(n) \quad \text{with} \quad \rho_0 = \rho_{\rm r}. \tag{2.106}$$

We see that the two distributions are identical, including the short-time fluctuations appearing for $n < n_r^* = n^*$. The key observation is then that any *recurrence problem*

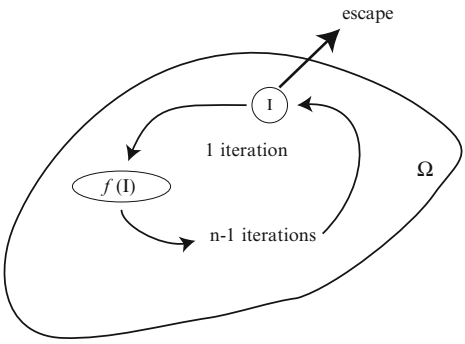


**Fig. 2.22** Illustration of the equivalence between recurrence and escape times

*can be considered as a leaked problem* with the special initial condition $\rho_0 = \rho_r$ (2.105).

The average lifetime is then given by Kac's formula (2.103) $\tau = 1/\mu(I)$. For finite $I$ it deviates *considerably* from the mean lifetime estimated according to (1.7) as $1/\kappa = -1/\ln[1-\mu_c(I)]$, which contains the c-measure of the leak. The reason for the large deviation is that $\rho_r$ in (2.105) is *atypical* from the point of view of the c-measure that concentrates along the unstable manifold of the chaotic saddle, i.e., it contains points that never escape under the backward dynamics, while all points associated with $\rho_r$ come from the leak.

It has been observed that different recurrence/leak regions of the same natural measure can lead to quite different exponential decays, particularly if an unstable periodic orbit of low period falls into $I$ [3, 16, 103, 571]. According to (2.104), there is a common phenomenon behind these results. Say there is a periodic orbit of period $n_p$ in $I$. We then expect a high recurrence probability $p_r(k = n_p)$. Since the average recurrence time is fixed and given by (2.103), the probabilities of other recurrence times $k \neq n_p$ are lower, leading to a reduced decay rate. In the context of leaked systems, the anomalously low escape rate is due to the significant overlaps between the leak and its preimages.